# Magnetic hollow buoyant alginate beads achieving rapid remediation of oil contamination on water

*by* Mochamad Zakki Fahmi

**Submission date:** 01-Sep-2021 08:58PM (UTC+0800)
**Submission ID:** 1639432069
**File name:** A38-MagneticHollowBuoyant.pdf (1.18M)
**Word count:** 10862
**Character count:** 56780

Journal of Environmental Chemical Engineering 9 (2021) 104935

Contents lists available at ScienceDirect

Journal of Environmental Chemical Engineering

journal homepage: www.elsevier.com/locate/jece

# Magnetic hollow buoyant alginate beads achieving rapid remediation of oil contamination on water

Satya Candra Wibawa Sakti [a,b,*], Rizki Ainuna Wijaya [a], Nindayu Indrasari [a], Mochamad Zakki Fahmi [a,b,*], Alfa Akustia Widati [a,b], Abdulloh [a,b], Nuryono [c], Chun-Hu Chen [d]

[a] Department of Chemistry, Faculty of Science and Technology, Universitas Airlangga, Campus C, Mulyorejo, Surabaya 60115, Indonesia
[b] Supramodification Nano-Micro Engineering Research Group, Universitas Airlangga, Campus C, Mulyorejo, Surabaya 60115, Indonesia
[c] Department of Chemistry, Faculty of Mathematics and Natural Sciences, Universitas Gadjah Mada, Sekip Utara, Yogyakarta 55281, Indonesia
[d] Department of Chemistry, National Sun Yat-sen University, Kaoshiung 80424, Taiwan

ARTICLE INFO

Editor: Dr. GL Dotto

*Keywords:*
Oil spill
Alginate
Magnetite
Graphene oxide
Buoyant
Remediation

ABSTRACT

Oil spills are a worldwide concern because of their negative impact on the environment. Thus, the development of simple yet effective methods for oil pollution remediation remains a significant global challenge. Of remediation techniques for oil removal, those involving adsorption are superior, but most reported adsorbents sink in water and are, consequently, difficult to collect after adsorption, generating secondary pollution. Thus, we developed magnetic maleic anhydride–alginate graphene oxide hollow beads (GO-MAGB-MA). Here, we report the characterization of GO-MAGB-MA, involving scanning electron microscopy, energy dispersive X-ray spectrometry, Raman spectroscopy, Fourier transform infrared spectroscopy, thermogravimetric analysis, and vibrating sample magnetometry. The experimental data fit the pseudo-second order kinetic model, having a chi-squared ($\chi^2$) $\leq$ 0.0069, average relative error (ARE) $\leq$ 0.4094, and coefficient of determination ($R^2$) $\geq$ 0.9998, and the Freundlich isotherm, having $\chi^2 \leq 3.33 \times 10^{-4}$, ARE $\leq$ 0.2349, and $R^2 \geq$ 0.9966, indicating that removal of oil was the rate-limiting step on heterogenous multilayer system. In comparison with other previous reported adsorbents, the GO-MAGB-MA shows superiority in term of adsorption process which was pH independent, rapid equilibrium adsorption and high adsorption capacity. GO-MAGB-MA also remained buoyant and magneto-responsive during adsorption process made it easy to be-recollected and regenerated while other reported adsorbents tend to sink during adsorption, and difficult to be re-recollected and ended as secondary pollutants. For future application, Combination with other technologies such as skimmer and continuous column adsorption experiment can be conducted for larger-scale oily water remediation.

## 1. Introduction

The release of oil-contaminated water into the marine environment by human activities or natural disasters causes long-term environmental catastrophes. To minimize the detrimental effects of oil spills on the environment and economy, immediate action is required. The risk of oil spills has increased as the exploration, transportation, and consumption of petroleum have grown, and serious contamination of the marine environment and aquatic biota has occurred. In March 1989, grounding of the Exxon Valdez (an oil tanker owned by Exxon Shipping Company) resulted in the contamination of the Prince William Sound with at least 35,500 t of crude oil that eventually spread to the Gulf of Alaska area [1]. In 2010, the Deepwater Horizon accident contaminated the Gulf of Mexico with around 500,000 $m^3$ of crude oil, making it the second largest oil spill disaster after the Gulf War (1991) crude oil spill in the Persian Gulf, Kuwait [2,3].

A key problem is that untreated oil spills spread rapidly in the aquatic environment, resulting in contamination over a large area. Chemically, petroleum oil consists of straight and branched hydrocarbons, polycyclic aromatic hydrocarbons, porphyrins, tar, and wax, which cause various levels of toxicity to humans and marine environments, including cytotoxicity, carcinogenicity, genotoxicity, and teratogenicity [4]. The layer of oil also forms a barrier that prevents sunlight and $O_2$ from penetrating deeper areas of water, which can disturb

* Corresponding authors at: Department of Chemistry, Faculty of Science and Technology, Universitas Airlangga, Campus C, Mulyorejo, Surabaya 60115, Indonesia.
*E-mail addresses:* satya.sakti@fst.unair.ac.id (S.C.W. Sakti), m.zakki.fahmi@fst.unair.ac.id (M.Z. Fahmi).

https://doi.org/10.1016/j.jece.2020.104935
Received 22 October 2020; Received in revised form 5 December 2020; Accepted 9 December 2020
Available online 13 December 2020
2213-3437/

photosynthesis and plant growth.

Consequently, environmental scientists have attempted to develop technology to reduce the catastrophic impact of oil spills. Remediation technologies, including bioremediation [5], chemical dispersants [6], booms and skimmers [7,8], in situ burning [9], and adsorption [10,11] have been reported. Among them, adsorption is the most applicable technique because of its excellent adsorption capacity, simplicity, and cost-effectiveness. Adsorption techniques is reported as an effective method not only for oil removal but also for other types of pollutant such as heavy metal ion [12,13] and dyes [14]. A high removal rate can be achieved by placing an adsorbent in contact with the oil on the water surface. Several reports have described the development of conventional adsorbents for oil spill remediation, for example, chitosan [15], clay [16, 17] and char [18]. Furthermore, to reduce costs, bio-materials including rice husks and banana and orange peels have also been explored [19]. However, some adsorbents sink in water, preventing effective contact with the oil on the water surface and making post-treatment separation difficult, thus resulting in seabed contamination.

As a potential adsorbent, graphene oxide (GO) has received considerable interest considering its high thermal and mechanical stability, high surface area, and high adsorption site density. Generally, GO is prepared by the chemical oxidation of graphite, as reported by Hummer and Offeman [20], whose technique was subsequently optimized by changing the reaction time, temperature, chemicals, or routes [21–24]. GO is an amphiphilic substance because of its (i) hydrophilic oxygen-bearing moieties, including hydroxyl, epoxy, and carboxyl groups, at the edges and basal layers and (ii) hydrophobic polyaromatic of unoxidized benzene rings. This amphiphilicity enables GO to interact with various pollutants, making it suitable for water desalination [25] and the removal of heavy metal ions, dyes [26], and organic toxic and hazardous substances [27]. Despite its advantages, the intense inter-layer attraction results in the agglomeration and restacking of GO. Moreover, post-adsorption collection is challenging. This is achieved conventionally by filtration or centrifugation, but these techniques are not feasible for large scale contamination. However, the magnetic separation of adsorbent has been highlighted as a promising solution.

The introduction of magnetic particles such as $Fe_3O_4$ to conventional adsorbents endows magnetic properties. $Fe_3O_4$ is a common soft magnetic material, being easily magnetized and demagnetized. Structurally, in $Fe_3O_4$, half the $Fe^{3+}$ ions fill the tetrahedral sites and the other half of the $Fe^{3+}$ ions join with $Fe^{2+}$ to occupy octahedral sites, forming an inverse spinel crystal structure with cubic symmetry. $Fe_3O_4$ can be synthesized by hydrothermal methods, thermal decomposition, and co-precipitation, but the latter technique is the most common because of its simplicity. Crucially, $Fe_3O_4$-based magnetic adsorbents are promising because of their magnetic properties and have been extensively used for the detoxification of polluted water; in particular, they have short separation time and do not generate secondary pollution [28–31]. Further, regeneration is favorable because loss of the magnetic adsorbent is avoided.

$Fe_3O_4$-based adsorbents can also be encapsulated in a polymeric matrix to prevent oxidation, which leads to the loss of magnetic properties, and increase adsorption [17,30,32–34]. Furthermore, dissolution of $Fe_3O_4$ in an acidic environment during adsorption can be avoided because of the protective matrix.

Alginate consists of a homopolymer unit of 1,4-connected (α-L-guluronic acid) (G block) and (β-D-mannuronic acid) (M block) and can be extracted from brown algae cell walls [35] or synthesized by bacteria [36]. The carboxylic groups of alginate can be crosslinked with divalent ions formed a unique "egg-box" like structure hydrogel with biocompatible, nontoxic, and biodegradable features [37]. These properties make alginate and alginate-based materials attractive for adsorbent preparation. In particular, the free carboxyl and hydroxyl groups on G and M blocks are responsible for electrostatic and complexation interactions with various toxic substances. Alginate is a natural polysaccharide that is suitable for $Fe_3O_4$ encapsulation.

**Table 1**
Chemical composition of artificial seawater.

| Component | Concentration ($g\ L^{-1}$) | Component | Concentration ($g\ L^{-1}$) |
|---|---|---|---|
| NaCl | 22.1 | NaF | $3 \times 10^{-3}$ |
| $MgCl_2{\cdot}6H_2O$ | 9.9 | LiCl | $1 \times 10^{-3}$ |
| $CaCl_2{\cdot}2H_2O$ | 1.5 | KI | $8.1 \times 10^{-5}$ |
| $Na_2SO_4$ | 3.9 | $MnCl_2{\cdot}4H_2O$ | $6 \times 10^{-7}$ |
| KCl | 0.61 | $CoCl_2{\cdot}6H_2O$ | $2 \times 10^{-6}$ |
| $NaHCO_3$ | 0.19 | $AlCl_3{\cdot}6H_2O$ | $8 \times 10^{-6}$ |
| KBr | $9.6 \times 10^{-2}$ | $FeCl_3{\cdot}6H_2O$ | $5 \times 10^{-6}$ |
| $Na_2B_4O_7{\cdot}10H_2O$ | $7.8 \times 10^{-2}$ | $Na_2WO_4{\cdot}2H_2O$ | $2 \times 10^{-6}$ |
| $SrCl_2$ | $1.3 \times 10^{-2}$ | $(NH_4)_6Mo_7O_{24}{\cdot}4H_2O$ | $1.8 \times 10^{-5}$ |

Herein, floating magnetic alginate–GO hollow beads were prepared via simple ionic gelation in the presence of $Ca^{2+}$ as a crosslinker and $CaCO_3$ and $NaHCO_3$ as cavity templates, followed by modification with maleic anhydride (MA), yielding a magnetic adsorbent for surface oil removal. GO-MAGB-MA showed efficient removal performance because of its flotation, which increased direct solid–liquid contact with the oil layer on the water surface. Static batch adsorption experiments were carried out to investigate the effects of contact time and initial pH and oil concentration on oil adsorption in freshwater and seawater. Several isothermal and kinetic models were used to fit the experimental data and determine the removal mechanism. The flotation and adsorption–desorption stability were also assessed to evaluate suitability for real oil-contaminated seawater remediation. The floating magnetic alginate–GO hollow beads modified with maleic anhydride remained floating for 30 days, were easily collected with an external magnet, and removed oil from seawater for 20 adsorption–desorption without loss in adsorptive performance, floatability, or magnetic collectability. Based on our knowledge, the study of self-floating alginate-based magnetic adsorbents has not been conducted for the removal of oil from the surface of seawater. The buoyancy, collectability, recyclability, and magneto-responsiveness are key features of GO-MAGB-MA that make it an attractive adsorbent for oil-contaminated water remediation in comparation with other reported adsorbents. This report will also provide easy method on removal of oil from the surface of freshwater and seawater simply by applying magnetic field.

## 2. Materials and methods

### 2.1. Materials

Pro-analysis grade materials were applied in this experiment without any additional purification. Sodium alginate ($Na(C_6H_6O_6)_n$, 300–400 cP), sodium bicarbonate ($NaHCO_3$, 99.7%), hydrochloric acid (HCl, 37%), acetic acid ($CH_3COOH$, 98%), sodium hydroxide (NaOH, 97%), phosphorus pentoxide ($P_2O_5$, 99%), potassium permanganate ($KMnO_4$, > 99%), and acetone ($C_3H_6O$, 99.5%) were obtained from Sigma-Aldrich, Germany. Maleic anhydride ($C_4H_2O_3$, 99%), calcium chloride ($CaCl_2{\cdot}2H_2O$, 100%), ethanol ($C_2H_5OH$, 97%), and sulfuric acid ($H_2SO_4$, 98%) were purchased from Merck, Germany. Magnetite ($Fe_3O_4$) was obtained from Kishida Chemical Co., Ltd. (Japan). Graphite flakes were supplied by Alfa Aesar (Taiwan), and calcium carbonate ($CaCO_3$, 99.5%) was purchased from Wako (Japan). Hexane ($C_6H_{14}$, 99%) was supplied by Fulltime (China). Crude oil with $\rho$ value of 0.7973 and $\eta$ value of 0.88 cP was used as adsorbate in adsorption experiments. Artificial seawater was prepared by dissolving seawater salt (Marine Art SF-1, Tomita Pharmaceutical Co.,Ltd, Japan) in deionized water and its chemical composition is presented in Table 1.

### 2.2. Entrapment of GO in floating magnetic alginate gel hollow beads

GO was obtained by the exfoliation of graphite in "preformed acidic oxidizing medium" (PAOM), as reported previously [38]. GO was added

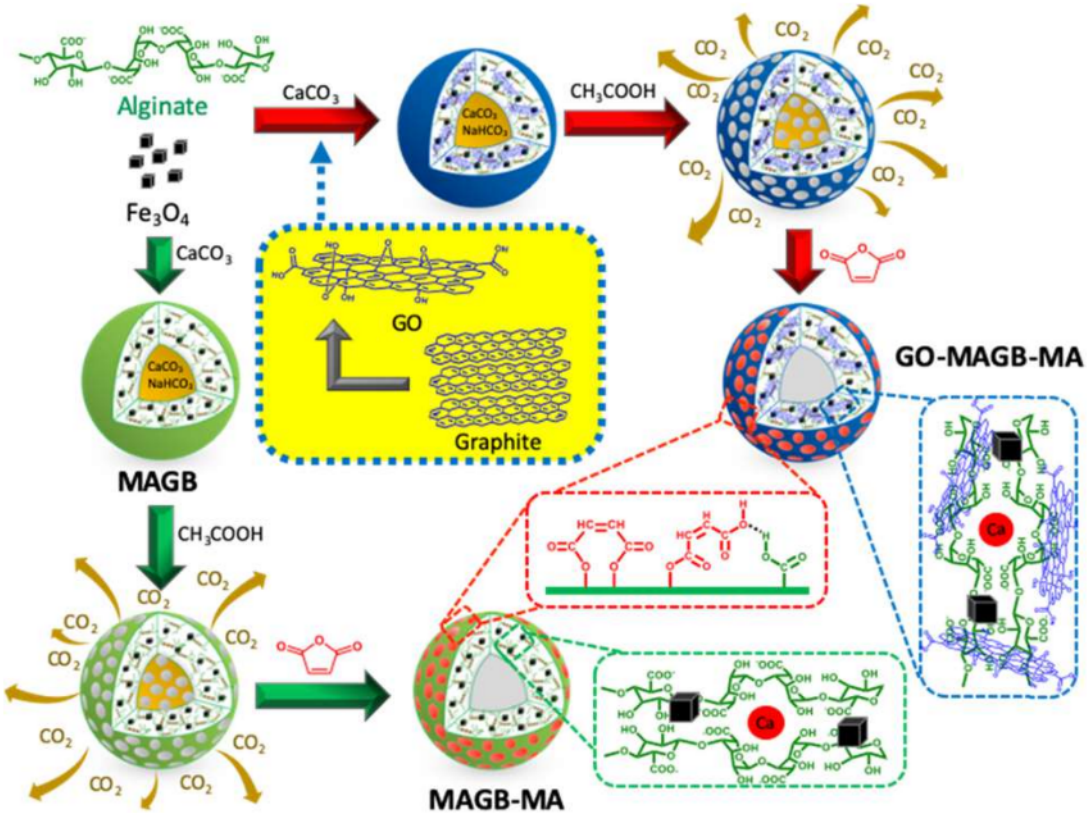


**Scheme 1.** Schematic illustration of preparation of maleic anhydride-alginate hollow bead reinforced with $Fe_3O_4$ and graphene oxide.

to deionized water and sonicated for 4 h to obtain a GO dispersion. Sodium alginate powder (0.75 g) was dissolved in 50 mL of deionized water at room temperature with continuous stirring until all was dissolved. The GO dispersion, magnetite, $NaHCO_3$, and $CaCO_3$ were added to the sodium alginate solution and mixed until homogeneous. The resulting black, viscous suspension was then left at room temperature overnight to remove trapped air bubbles. The suspension was forced through a micropipette tip into 500 mL of 5 wt% $CaCl_2$ solution, maintained for 24 h with gentle stirring, and washed with demineralized water several times. The obtained black beads were then immersed in 300 mL of 6% $CH_3COOH$ solution overnight and washed with demineralized water several times. The product is GO-MAGB. MAGB was synthesized in a similar manner without the addition of GO addition.

### 2.3. Anchoring of the maleic anhydride moiety

GO-MAGB-MA was prepared by placing GO-MAGB in contact with MA in acetone. Briefly, GO-MAGB was immersed in acetone with gentle stirring overnight to remove water inside the beads. The acetone-washed GO-MAGB was then immersed in gently stirred 0.05 M maleic anhydride in acetone solution for 30 min. The temperature of the mixture was then increased to 50 °C and maintained at this temperature for 3 h to complete the esterification reaction. Finally, the beads were washed with acetone, ethanol, and demineralized water and lyophilized. MAGB-MA was prepared in a similar manner using MAGB instead of GO-MAGB. The preparation of GO-MAGB and its modification with MA are illustrated in Scheme 1.

### 2.4. Methods

X-ray diffraction analysis of GO was performed using X-ray diffractometry (X-Pert MPD, Philips, Germany) from $2\theta = 5°$ to 90° at 5 ° $min^{-1}$ with Cu-$K_\alpha$ radiation ($\lambda = 1.54443$ Å). Raman spectra were recorded at a wavelength of 532 nm on a Raman spectrometer (InVia Raman, Renishaw, UK). The thickness of the prepared GO sheets was measured using atomic force microscopy (AFM, Dimension Icon, Bruker, Germany) in ScanAsyst mode. The morphology was investigated using scanning electron microscopy (SEM, FlexSEM-1000, Hitachi, Japan), energy dispersive X-ray spectroscopy, and transmission electron microscopy (TEM, JEM-1400 JEOL, Japan). The magnetic properties of magnetic beads were examined under a magnetic field ranging from −8000 to 8000 Oe at room temperature on a vibrating sample magnetoanalyzer (Lake Shore 7400 series, USA). The bead size was measured using a digital caliper (Krisbow, Indonesia). Functional groups were identified by Fourier transform infrared (FTIR) spectroscopy (IRTracer-100, Shimadzu, Japan) using the KBr disk method from 4000 to 400 $cm^{-1}$ with resolution 4 $cm^{-1}$. The thermal stability was determined using thermogravimetric analysis (TGA, TGA-4000, Perkin Elmer, USA). For these measurements, the samples were heated under continuous flow of $N_2$ at a heating rate of 5 °C $min^{-1}$ to 900 °C.

### 2.5. Swelling and flotation

For the swelling tests, a gram of lyophilized magnetic hollow bead was soaked in freshwater and seawater for 24 h. The swelled beads were collected using a magnet. The diameter before and after soaking were recorded. Flotation experiments were conducted by soaking 50 of

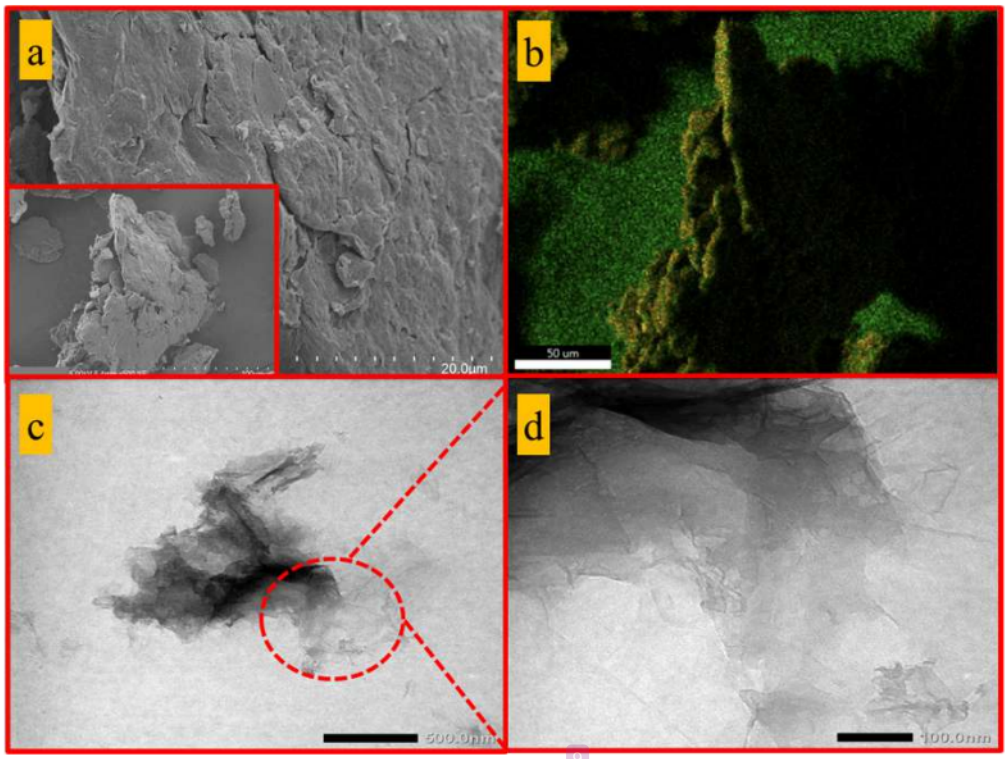


**Fig. 1.** (a) SEM image (inset: low magnetization image), (b) EDX elemental mapping, (c) Low magnification TEM image, (d) High magnification TEM image.

lyophilized magnetic hollow beads in freshwater and seawater for 30 d. The swelling degree (SD) and flotation degree (FD) of the magnetic hollow beads were calculated using Eqs. (1) and (2).

$$SD\% = \frac{\phi_w - \phi_d}{\phi_d} \times 100 \quad (1)$$

$$FD\% = \frac{n_{30}}{n_0} \times 100 \quad (2)$$

Here, $\phi_w$ and $\phi_d$ are the diameters of the wet and dry magnetic hollow beads, respectively, and $n_0$ and $n_{30}$ are the numbers of floating beads at the start and after 30 d. For accuracy, swelling and flotation experiments were conducted in triplicate.

### 2.6. Use and reusability

Batch adsorption experiments of oil-contaminated freshwater and seawater was performed by placing 0.015 g of MAGB, MAGB-MA, or GO-MAGB-MA in contact with 15 mL deionized water or seawater containing 66.67 g $L^{-1}$ of oil. The influence of initial pH was examined by regulating the pH of the water–oil mixture with 0.01 mol $L^{-1}$ NaOH or HCl solution. For the analysis of the removal kinetics, the contact time with the water–oil mixture varied from 5 to 120 min. The adsorption data were then simulated with non-linearized pseudo-first order (PFO), pseudo-second-order (PSO), Elovich, and linear intraparticle diffusion (IPD) kinetic models. The adsorption isothermal behavior was studied with oil concentrations ranging from 40 to 120 g $L^{-1}$, and the Freundlich, Langmuir, Sips, and Redlich–Peterson (R–P) isotherms were employed to evaluate the adsorption data. The adsorption capacities of MAGB, MAGB-MA, and GO-MAGB-MA at equilibrium ($q_e$, g of oil/g of adsorbent) were computed using Eq. (3).

$$q_e = \frac{(m_0 - m_e)}{m_a} \quad (3)$$

Here, $m_0$ and $m_e$ are the initial oil mass and equilibrium oil mass in solution (g), respectively, and $m_a$ is the mass (g) of MAGB, MAGB-MA, or GO-MAGB-MA.

To estimate the reusability of the spent MAGB, MAGB-MA, and GO-MAGB-MA, beads were loaded with oil in 20 mL of a mixture of 100 g $L^{-1}$ of oil in deionized water or seawater at pH 6 equilibrated on a mechanical shaker at room temperature for 2 h at 100 rpm. The oil-loaded beads were collected using a magnet and treated with *n*-hexane. Subsequently, the regenerated beads were sonicated in hexane, ethanol, and water several times before the next cycle. The regeneration of MAGB, MAGB-MA, and GO-MAGB-MA was carried out over 20 adsorption–desorption cycles in deionized water or seawater.

## 3. Results and discussion

### 3.1. Physical characteristics of as-prepared GO

The morphology and topography of GO were observed using SEM-EDX, and TEM. As shown in Fig. 1, the obtained GO has an irregular, layer-like shape with a wrinkled surface. EDX analysis, as can be seen in Fig. 1(b), revealed the elemental composition of GO to be 47% carbon and 53% oxygen. No trace elements were detected. A high oxygen/carbon ratio indicates the presence of oxygen-bearing functional groups on the surface of the carbon structure. A high oxygen content affects the folding of the GO layers, as shown in the TEM micrograph (Fig. 1(c, d)). TEM analysis confirmed the thin layer structure, which is visible as a transparent area. The darker area corresponds to stacked or folded GO layers induced by the high content of oxygen, as quantified by EDX

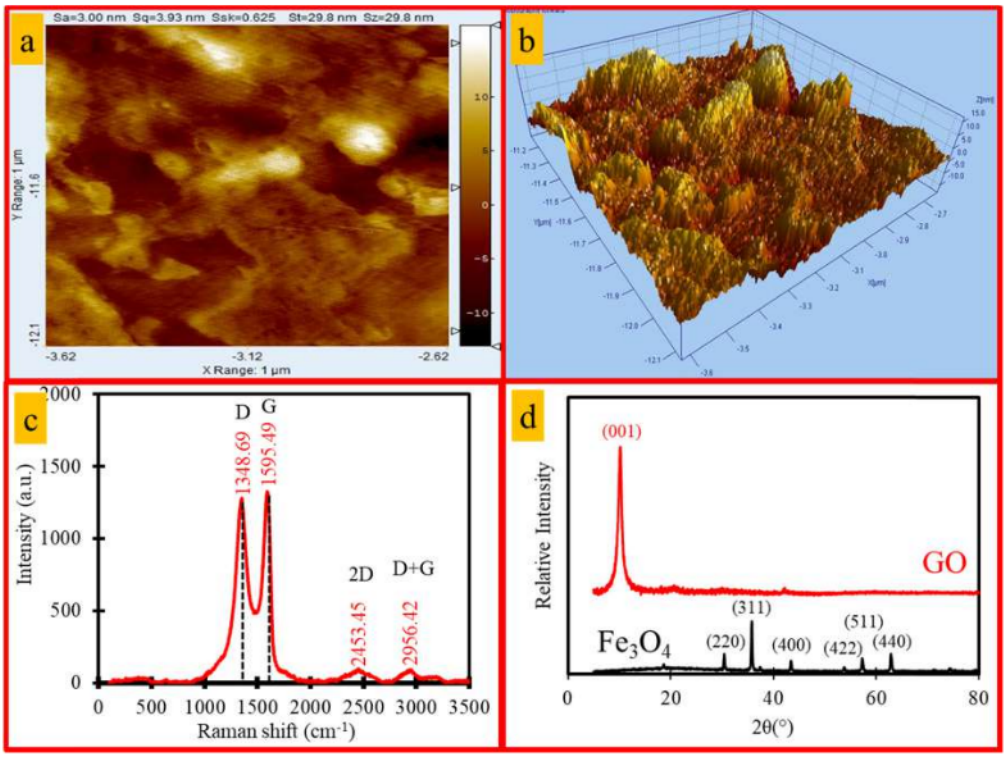


**Fig. 2.** (a) AFM image, (b) 3D-AFM image (c) Raman spectra of as-prepared graphene oxide and (d) X-ray diffractogram of GO and $Fe_3O_4$.

analysis. The morphology and topography of GO were then further analyzed using AFM, and the results are presented in Fig. 2(a, b). The 3D-AFM micrograph shows that the maximum height of GO was 8 nm, and it was relatively flat.

Fig. 2(c) shows the Raman spectra of GO, showing the D, G, 2D, and D + G bands at 1348.69, 1595.49, 2543.45, and 2956.42 $cm^{-1}$, respectively. The D band corresponds to the $sp^3$-hybridized carbon bonds in GO arising from basal/edge defects or imperfection of its crystal structure, whereas the G band is associated with ordered $sp^2$-hybridized carbon bonds in hexagonal graphitic structures such as graphene and its derivatives. The 2D band indicates agglomeration or stacking of GO layers. The defects in the as-prepared GO can be estimated from the ratio of the G and D band intensities ($I_D/I_G$) We obtained a value of 0.956, which suggests that the as-prepared GO has many defects in the layers.

X-ray diffractometry was used to determine the crystal structure of the obtained $Fe_3O_4$ and GO. As shown in Fig. 2(d), diffraction peaks associated to (220), (311), (400), (422), (511) and (440) plane are observed in diffractogram which indicated $Fe_3O_4$ spinel with cubic structure (JCPDS, No 79-0418). A significant peak is detected at $2\theta = 10.02°$ (Fig. 1(f)), which corresponds to the GO (001) plane. The diffraction peak at $2\theta = 10.02°$ indicates intraplanar spacing and crystallite size of 0.8992 and 2.1782 nm, respectively. The number of GO layers was found to be 2 or 3, suggesting stacked layers, as confirmed by TEM and AFM.

### 3.2. SEM and EDX analysis of GO-MAGB-MA

The magnetic alginate hollow beads were synthesized using $CaCO_3$ and $NaHCO_3$ as the cavity template. The carbonates were dispersed in an alginate solution containing $Fe_3O_4$ or a combination of $Fe_3O_4$ and GO. After the $Ca^{2+}$ crosslinking step, carbonates were removed from the beads by immersion in weak acid, leaving a hollow structure, as shown by the reactions in Eqs. (4) and (5).

$$CaCO_3 + CH_3COOH \rightarrow (CH_3COO)_2Ca + H_2O + CO_2 \quad (4)$$

$$NaHCO_3 + CH_3COOH \rightarrow CH_3COONa + H_2O + CO_2 \quad (5)$$

Acetic acid was used instead of a strong acid to prevent the dissolution of $Fe_3O_4$. Initially, the beads sank, but, after carbonate removal, they floated to the surface. Thus, the formation of an internal cavity resulted in buoyant magnetic alginate beads. The preparation method is illustrated in Scheme 1.

The average diameters of the as-prepared MAGB, MAGB-MA, and GO-MAGB-MA beads are presented in Table 2. The incorporation of GO, followed by MA modification, slightly increased the bead diameter compared to those of the bare magnetic alginate hollow beads (MAGB). The microstructures of the MAGB, MAGB-MA, and GO-MAGB-MA beads

**Table 2**
Average bead size and magnetic-physical properties of MAGB, MAGB-MA and GO-MAGB-MA.

| Magnetic Adsorbent | Component | Average Bead Size (mm) | Hc (G) | Ms (emu $g^{-1}$) | Mr (emu $g^{-1}$) |
|---|---|---|---|---|---|
| MAGB | Alginate, $Fe_3O_4$ | 2.93 ± 0.18 | 129.35 | 43.268 | 5.314 |
| MAGB-MA | Alginate, $Fe_3O_4$, maleic anhydride | 3.02 ± 0.23 | 125.4 | 43.134 | 5.134 |
| GO-MAGB-MA | Alginate, $Fe_3O_4$, maleic anhydride, GO | 3.24 ± 0.16 | 121.2 | 26.371 | 3.192 |

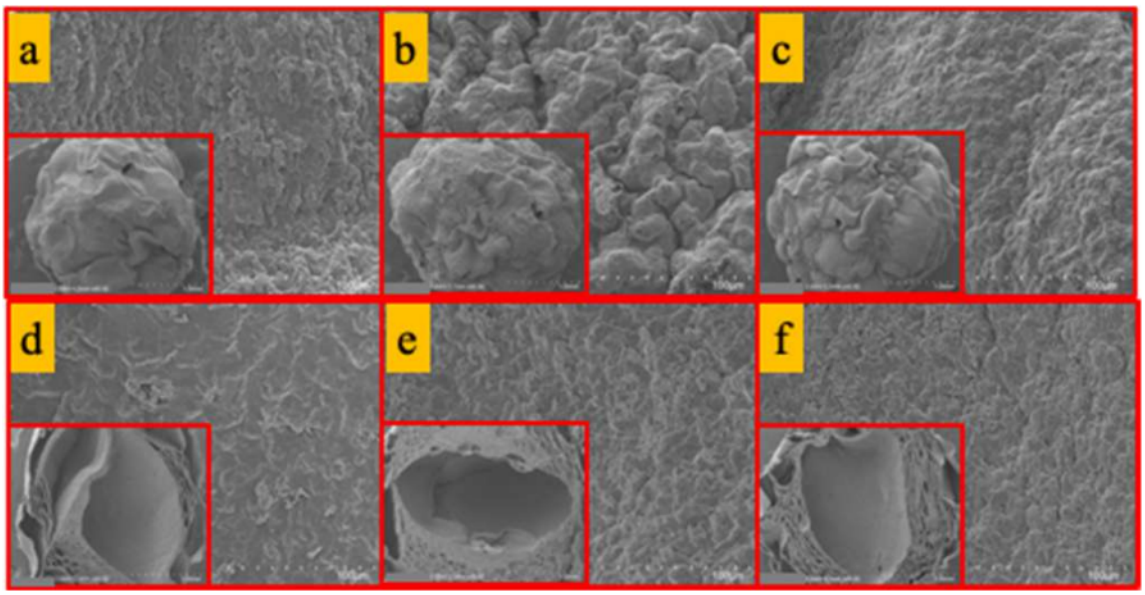


**Fig. 3.** Outer surface SEM image of (a) MAGB. (b) MAGB-MA (c) GO-MAGB-MA and inner surface SEM image of (d) MAGB (e) MAGB-MA (f) GO-MAGB-MA.

were studied by SEM analysis of individual lyophilized beads. The interior structure was evaluated by cutting the beads in half. Fig. 3 shows that MAGB has a smooth surface with folds, whereas MAGB-MA and GO-MAGB-MA have relatively rough surfaces, making them suitable for modification with MA and GO. Additional smaller cavities can also be observed in the interior of MAGB. In contrast, the walls of GO-MAGB-MA are denser, and there are fewer small cavities because of the presence of GO. EDX mapping analyses (Fig. 4) were carried out to obtain the elemental distribution. C, O, and Fe were detected in the outer and inner surfaces of MAGB, MAGB-MA, and GO-MAGB-MA. The carbon content on the surface of MAGB increased by approximately 1.5% after MA modification (MAGB-MA) and 2.4% after the incorporation of GO followed by MA modification. Although EDX analysis cannot distinguish the source of carbon (i.e., alginate, GO, or MA), the increased carbon content is likely a result of MA modification and GO incorporation. A signal corresponding to Ca was detected, indicating the presence of the crosslinker $Ca^{2+}$ and residual $Ca^{2+}$ from the dissolution of carbonates in the internal and external parts of the magnetic alginate hollow beads.

### 3.3. FTIR spectroscopy

Characterization of material and its derivatives by infrared spectroscopy is essential to be conducted in order to obtain information related to the presence of organic groups [39]. The synthesis of the magnetic alginate hollow beads, incorporation of GO, and modification with MA were confirmed from the FTIR spectra of $Fe_3O_4$, GO, MAGB, MAGB-MA, and GO-MAGB-MA between 4000 and 400 $cm^{-1}$. As shown in Fig. 5(a), in the spectrum of $Fe_3O_4$, a band at 3630 $cm^{-1}$ associated with the O–H stretching of physically adsorbed water molecules was observed. In addition, bands corresponding to Fe–O stretching in the tetrahedral and octahedral sites of spinel ferrite were observed at 584 and 445 $cm^{-1}$, respectively [68]. The FTIR spectrum of GO showed bands at 3603, 1739, 1602, and 1421 $cm^{-1}$, which can be assigned to O–H, carbonyl, epoxy C–O and the C=C $sp^2$ carbon network, and C–OH stretching vibrations, respectively. After the addition of alginate to $Fe_3O_4$, extra bands at 1627, 1427, and 1018 $cm^{-1}$ were observed. The bands at 1627 and 1427 $cm^{-1}$ are associated with the C=O stretching vibrations [40], and the C–O vibration of the pyranose ring appear at 1018 $cm^{-1}$, indicating the successful coating of $Fe_3O_4$ by alginate. The modification of MAGB resulting in MAGB-MA was confirmed by the appearance of bands at 1816 and 1739 $cm^{-1}$ associated with carbonyl symmetric and asymmetric stretches in MA. A similar pattern can also be observed in the FTIR spectra of GO-MAGB-MA with additional changes. The band at approximately 1600 $cm^{-1}$ in the FTIR spectra of GO-MAGB-MA associated with the C=O vibration of the –COOH group became stronger, indicating the formation of hydrogen bonds between the –COOH group of the alginate backbone and the –COOH group of GO.

### 3.4. Effect of GO and MA on thermal stability

Next, TGA/DTG of MAGB, MAGB-MA GO-MAGB, and GO-MAGB-MA was carried out and the results are presented in Fig. 5(b, c). The TGA/DTG curves of $Fe_3O_4$ is relatively constant from room temperature to 800 °C, indicating high thermal stability. In contrast, non-magnetic AGB lost most of its mass during heating. The TGA/DTG curves of MAGB, MAGB-MA, GO-MAGB, and GO-MAGB-MA are similar because of the shared alginate backbone.

Non-magnetic AGB decomposed around 10.62% at 192.7 °C of its mass because of water evaporation whereas MAGB and GO-MAGB lost around 7% of their masses at slightly higher temperature (196.88 °C). The MA-modified beads (MAGB-MA and GO-MAGB-MA) showed lower mass loss (only around 2%) at higher temperature (201.35 °C) than those of the unmodified beads (MAGB and GO-MAGB), suggesting that the MA moiety and GO increased the thermostability at this temperature. Around 20–22% of the masses of MAGB, MAGB-MA, GO-MAGB, and GO-MAGB-MA were lost in the second stage which is half that of AGB (around 47%) due to thermal-decomposition of alginate bead walls at 200–350 °C via pyranose ring opening, disintegration of the GO structure, and fragmentation of alginate–MA bonds [41]. The thermostability of $Fe_3O_4$ in MAGB, MAGB-MA, GO-MAGB, and GO-MAGB-MA is the main cause of this. At the carbonization stage, all beads lost 31–38% of their masses, whereas the non-magnetic AGB retained only 25% of its initial mass. The GO-containing beads (GO-MAGB and GO-MAGB-MA) showed smaller mass loss at this stage in comparison with the beads without GO addition (MAGB and MAGB-MA), indicating

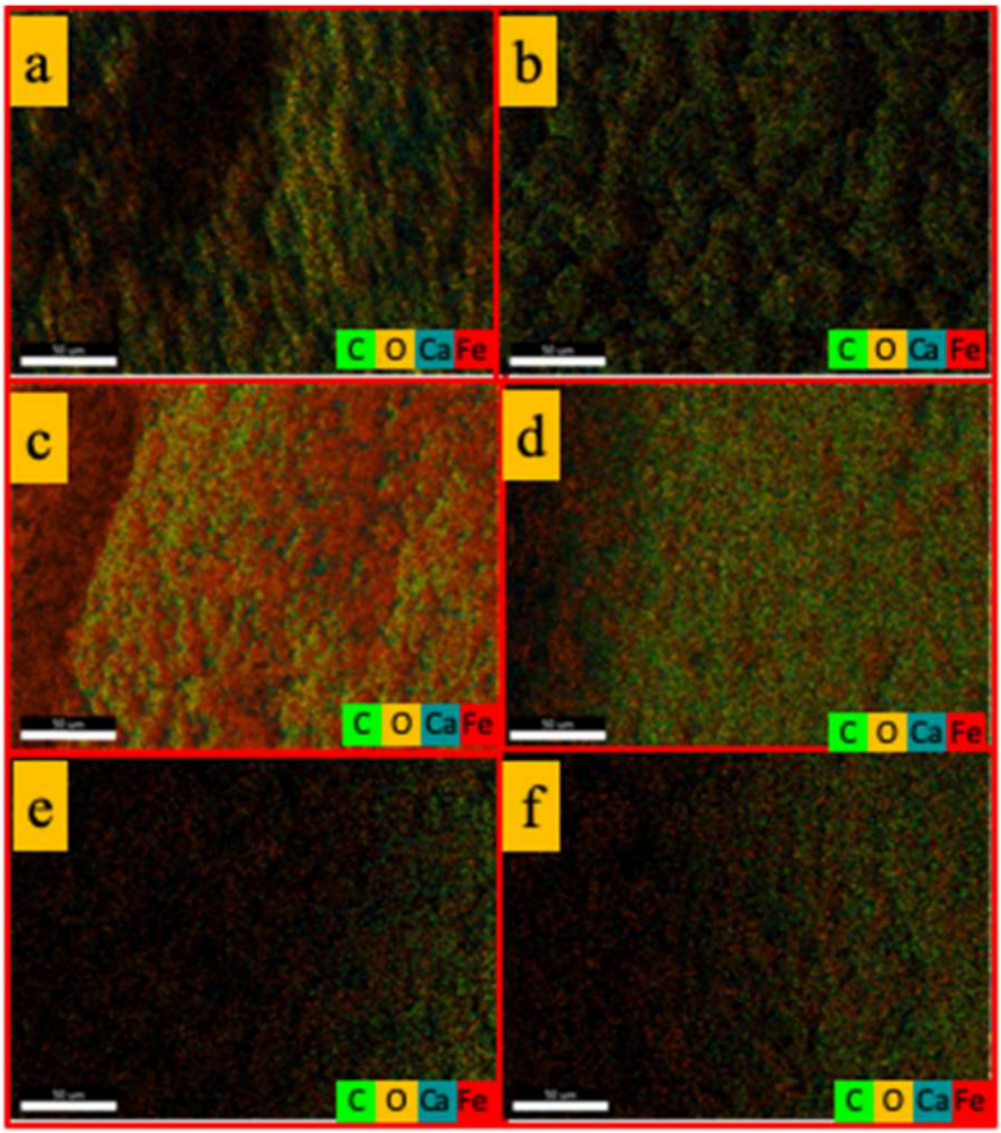


**Fig. 4.** Outer surface EDX mapping of (a) MAGB. (b) MAGB-MA (c) GO-MAGB-MA and inner surface EDX mapping of (d) MAGB (e) MAGB-MA (f) GO-MAGB-MA.

that GO increased thermostability at this temperature. The MAGB rapidly carbonized at 613.44 °C while GO-MAGB-MA carbonized at higher temperature (705.49 °C) which indicated that the GO-MAGB-MA was more thermally stable than GO-MAGB-MA The TGA/DTG results show that the obtained magnetic hollow beads are thermostable below 150 °C, which is compatible with real conditions.

### 3.5. Vibrating sample magnetometry analysis

Magnetization analysis was performed at 8000 Oe at room temperature, and the magnetization (M–H) curves and parameters of MAGB, MAGB-MA, and GO-MAGB-MA are shown in Fig. 6(a) and listed in Table 2, respectively. MAGB, MAGB-MA, and GO-MAGB-MA achieved magnetization saturation in the applied external magnetic field. The $M_s$ of GO-MAGB-MA is lower than those of MAGB and MAGB-MA because of the greater non-magnetic content in GO-MAGB-MA. Magnetite ($Fe_3O_4$) particles in the bead structure endow the magnetic behavior, whereas the alginate network, GO, and MA layers are non-magnetic and shield the $Fe_3O_4$ core, decreasing its magnetic performance in an applied magnetic field. However, MAGB, MAGB-MA, and GO-MAGB-MA were paramagnetic, enabling collection using an external magnetic field as shown in Fig. 6(b–d), as reported for other magnetic materials coated with various matrices [14,30,42,69].

### 3.6. GO- and MA-dependent swelling and self-floating properties

Generally, alginate-based hydrogels swell in water; therefore, we investigated the effect of modification with GO and MA on the swelling of beads. Bare magnetic hollow beads with no GO or MA swelled significantly in freshwater and more so in seawater. With increase in GO content, the SD decreased because GO restricted the movement of the alginate backbone in the bead structure, and modification with MA

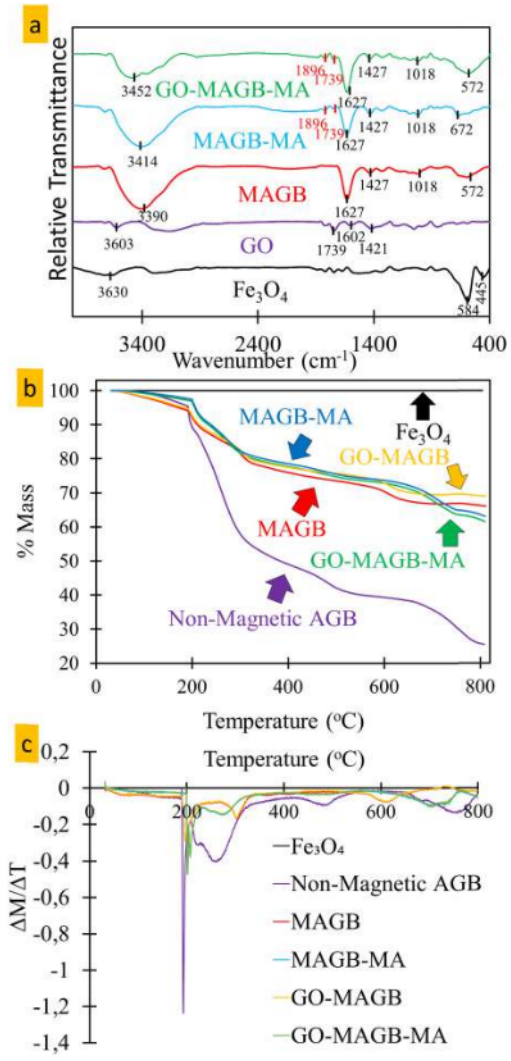


**Fig. 5.** (a) FTIR spectra, (b) thermogravimetric analysis curves, (c) derivative thermogravimetric analysis curves.

further decreased the SD because MA bridges the M and G blocks in alginate via ester formation, resulting in a rigid, stable bead structure. As shown in Fig. 6(e), magnetic hollow beads with low GO contents had higher SD values in seawater than in freshwater. A high concentration of $Na^+$ and other monovalent ions in seawater replace the $Ca^{2+}$ in the magnetic hollow beads by weakening the ion exchange mechanism and increasing bead size [43]. However, the addition of GO following MA modification can prevent such ion exchange by minimizing the movement of alginate and release of $Ca^{2+}$, resulting in unchanged bead size. Interestingly, magnetic hollow beads with 2–4% GO modified with MA remained floating after 30 days, unlike 0% and 1% GO beads, and most of the beads without GO and MA sank in the bottom of water as shown in Fig. 6(f). The addition of a higher content of GO followed by MA modification helps the magnetic hollow beads maintain their initial shape and size in freshwater and seawater; thus, excess swelling and collapse can be avoided. Thus, GO addition and MA modification improved the swelling and floating properties of magnetic hollow beads.

### 3.7. Oil adsorption performance

#### 3.7.1. Effect of pH

In oil spill remediation, the pH of the oil–water mixture has a strong impact on the adsorption efficiency, affecting not only the adsorption rate and capacity but also the adsorbent–mixture interface behavior. Thus, the amounts of oil adsorbed by MAGB, MAGB-MA, and GO-MAGB-MA at pH 3–10 at room temperature in freshwater and seawater were determined. As shown in Fig. 7(a, b), pH had little effect on oil adsorption by GO-MAGB-MA in freshwater and seawater, having a maximum adsorption capacity at pH 6; thus, the pH and salinity of water have little impact on the removal of oil, suggesting that non-electrostatic interactions are key to the removal mechanism. As shown in inset of Fig. 6(b–d), GO-MAGB-MA has a higher water contact angle in comparison with that of MAGB and MAGB-MA, demonstrating that GO-MAGB-MA is more hydrophobic than of MAGB and MAGB-MA. The non-oxidized basal plane of GO has been reported to attract oil through hydrophobic interactions [44]. Moreover, this interaction was improved by the presence of an MA layer in the beads. Thus, GO-MAGB-MA exhibited higher oil removal performance. This result indicates that the combination of GO and MA modification improved the adsorption capacity and pH tolerance of magnetic hollow beads in freshwater and seawater media. At pH > 10, the presence of a higher concentration of NaOH hydrolyzed oil by reaction with the acidic long hydrocarbon chain of oil. Therefore, to avoid saponification, adsorption at pH > 10 was not conducted.

#### 3.7.2. Effect of contact time

The effect of contact time on the removal of oil by MAGB, MAGB-MA, and GO-MAGB-MA in freshwater and seawater was investigated using batch adsorption experiments at contact times of 5–120 min. The initial shaking speed, pH, and initial oil concentration, were maintained at 100 rpm, 6, and 66.67 g $L^{-1}$, respectively. As shown in Fig. 7(c, d), the amount of oil adsorbed by MAGB, MAGB-MA, and GO-MAGB-MA in seawater increased rapidly and reached equilibrium within 30 min, and there was no significant increased oil removal from 30 to 120 min. In the initial stages of adsorption, there are a large number of binding sites for oil. As these sites are saturated with oil, the rate of adsorption falls and equilibrium is achieved, i.e., the flat area in Fig. 7(c, d). This behavior was also observed for MAGB, MAGB-MA, and GO-MAGB-MA in freshwater with no significant differences in adsorption capacity and equilibrium time. The time to equilibrium adsorption in freshwater and seawater was relatively short, making them promising agents for rapid oil adsorption.

#### 3.7.3. Initial oil concentration dependence

In addition to contact time, the initial oil concentration was varied to understand how equilibrium was reached, as well as to determine the adsorption capacities. Batch adsorption experiments were conducted at pH 6 and a shaking speed of 100 rpm using a 1 g $L^{-1}$ adsorbent dose. The initial oil concentration was 40–120 g $L^{-1}$, and, to ensure that equilibrium was achieved, a contact time of 120 min was selected (although 30 min are adequate based on kinetic analysis). As shown in Fig. 8, in the low oil concentration range, the removal of oil from seawater by GO-MAGB-MA increased steadily as the initial concentration of oil increased. At higher initial concentrations of oil, the adsorption capacity was reduced, and equilibrium was reached. A high ratio of vacant binding sites to oil molecules is responsible for the rapid increase in the adsorbed capacity of GO-MAGB-MA at low initial oil concentrations. At equilibrium, the binding sites were fully occupied, so the amount of oil adsorbed from the mixture became steady and no more oil molecules could be accommodated by GO-MAGB-MA. Because of the abundance of active binding sites, GO-MAGB-MA adsorbed more oil molecules than MAGB and MAGB-MA. Fig. 8 shows that the removal of oil in freshwater by MAGB, MAGB-MA, and GO-MAGB-MA followed a similar pattern, indicating that salinity had little effect on oil removal.

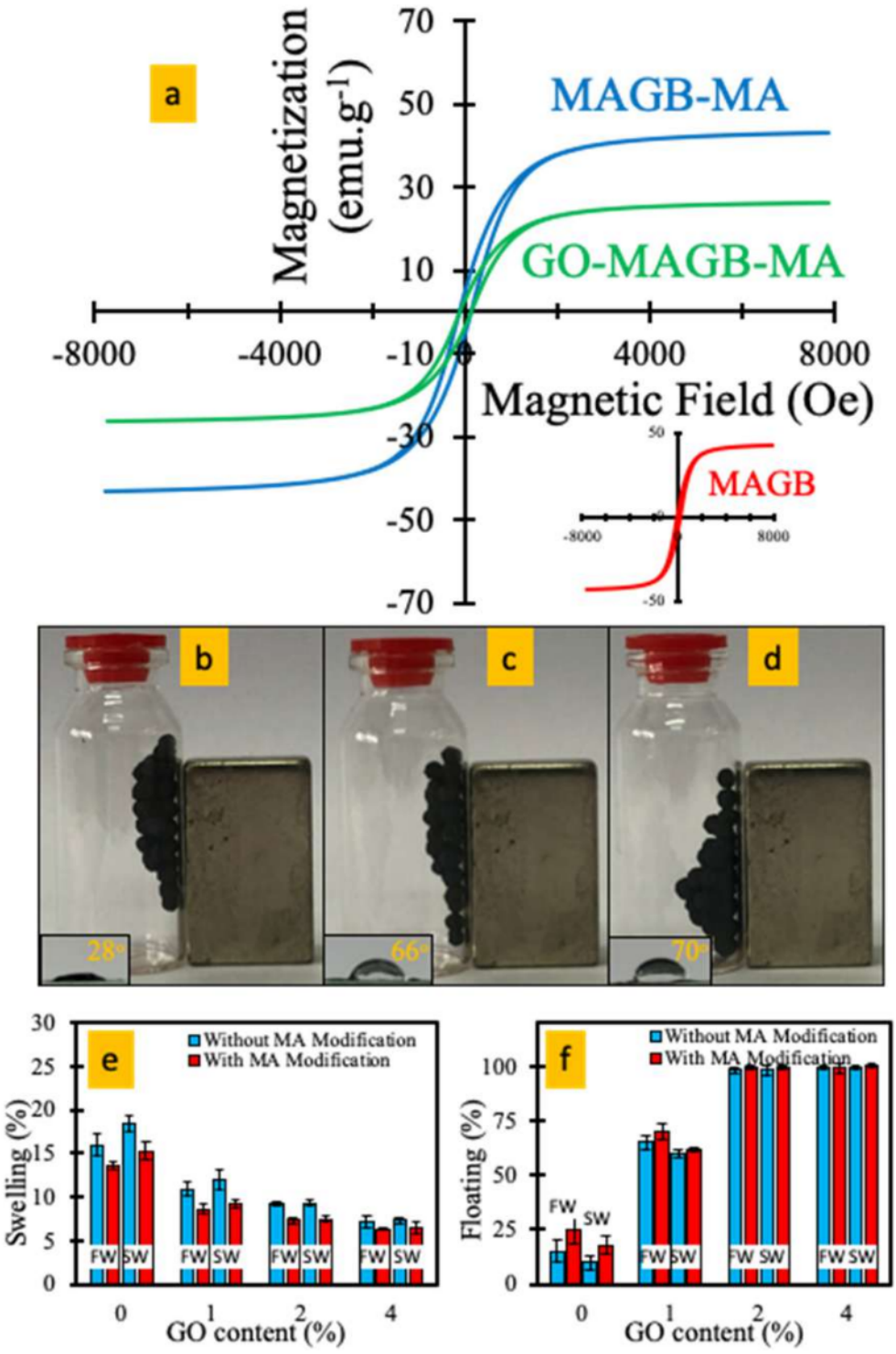


**Fig. 6.** (a) M–H magnetization curves of the MAGB, MAGB-MA and GO-MAGB-MA, images of (b) MAGB, (c) MAGB-MA and (d) GO-MAGB-MA attracted by magnet (inset: contact angle). Influence of GO content in magnetic alginate hollow beads on (e) swelling and (f) self-floating property.

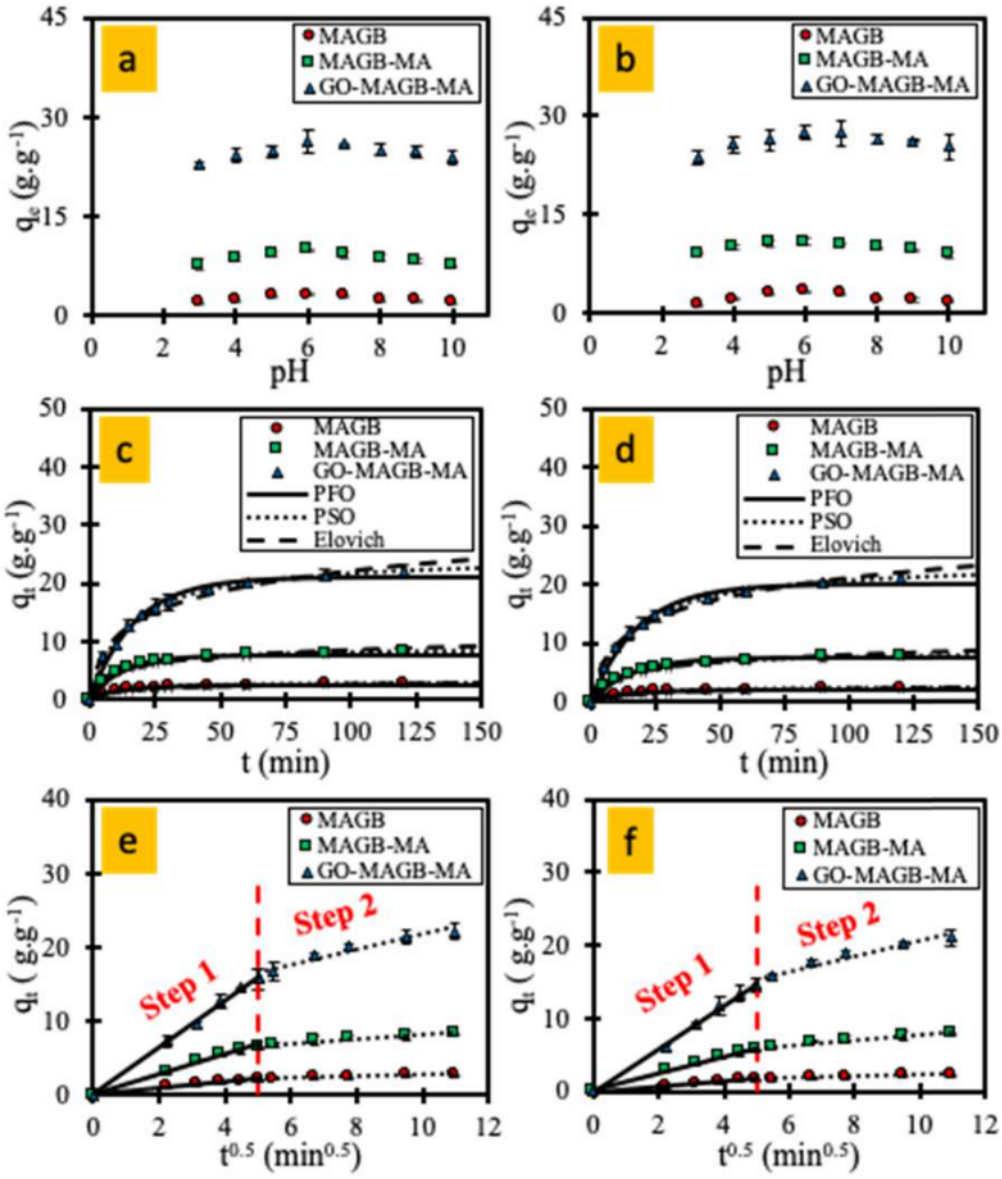


**Fig. 7.** Effect of initial pH on magnetic removal of oil by MAGB, MAGB-MA and GO-MAGB-MA in (a) freshwater and (b) seawater (experiment condition: $C_0$: 66.67 g L$^{-1}$, t: 2 h, T: 25 °C, adsorbent dose: 1 g L$^{-1}$ and n: 3), kinetics experimental data of MAGB, MAGB-MA, GO-MAGB-MA fitted with non-linearized PFO, PSO and Elovich model in (c) freshwater and (d) seawater, linear IPD fitting of experimental data in (e) freshwater and (f) seawater (experiment condition: $C_0$: 66.67 g L$^{-1}$, pH 6, T: 25 °C, adsorbent dose: 1 g L$^{-1}$ and n: 3).

*3.7.4. Kinetic modeling and effect of water type*

The adsorption kinetics is controlled by complex, simultaneous processes involving mass transfer, diffusion, and the formation of physico-chemical interactions. To determine the mechanism of oil adsorption by MAGB, MAGB-MA, and GO-MAGB-MA, four kinetic models were used: PFO [45], PSO [46], Elovich [47], and IPD [48].

The simulated data with non-linearized PFO, PSO, Elovich, and linear IPD kinetic model are shown in Fig. 7(c-f) and all obtained kinetic parameters are listed in Table 3. The fitting of experimental data obtained for oil adsorption in freshwater and seawater to the PSO and Elovich models resulted in high ARE and $\chi^2$ values and low $R^2$ values, demonstrating that neither model describes the oil adsorption mechanism by MAGB, MAGB-MA, and GO-MAGB-MA well. Contrarily, low ARE and $\chi^2$ and high $R^2$ values were obtained by fitting the experimental data to the PSO model, suggesting that adsorption is the rate-limiting step. As shown in Table 3, the $K_{PSO}$ for adsorption in seawater are only slightly different with $K_{PSO}$ obtained from adsorption in freshwater, implying that the water type gives insignificant impact on adsorption rate.

In the IPD studies (Fig. 7(e, f)), two-stage oil adsorption was observed for MAGB, MAGB-MA, and GO-MAGB-MA in freshwater and seawater. First, there is a rapid adsorption rate resulting in a sharp

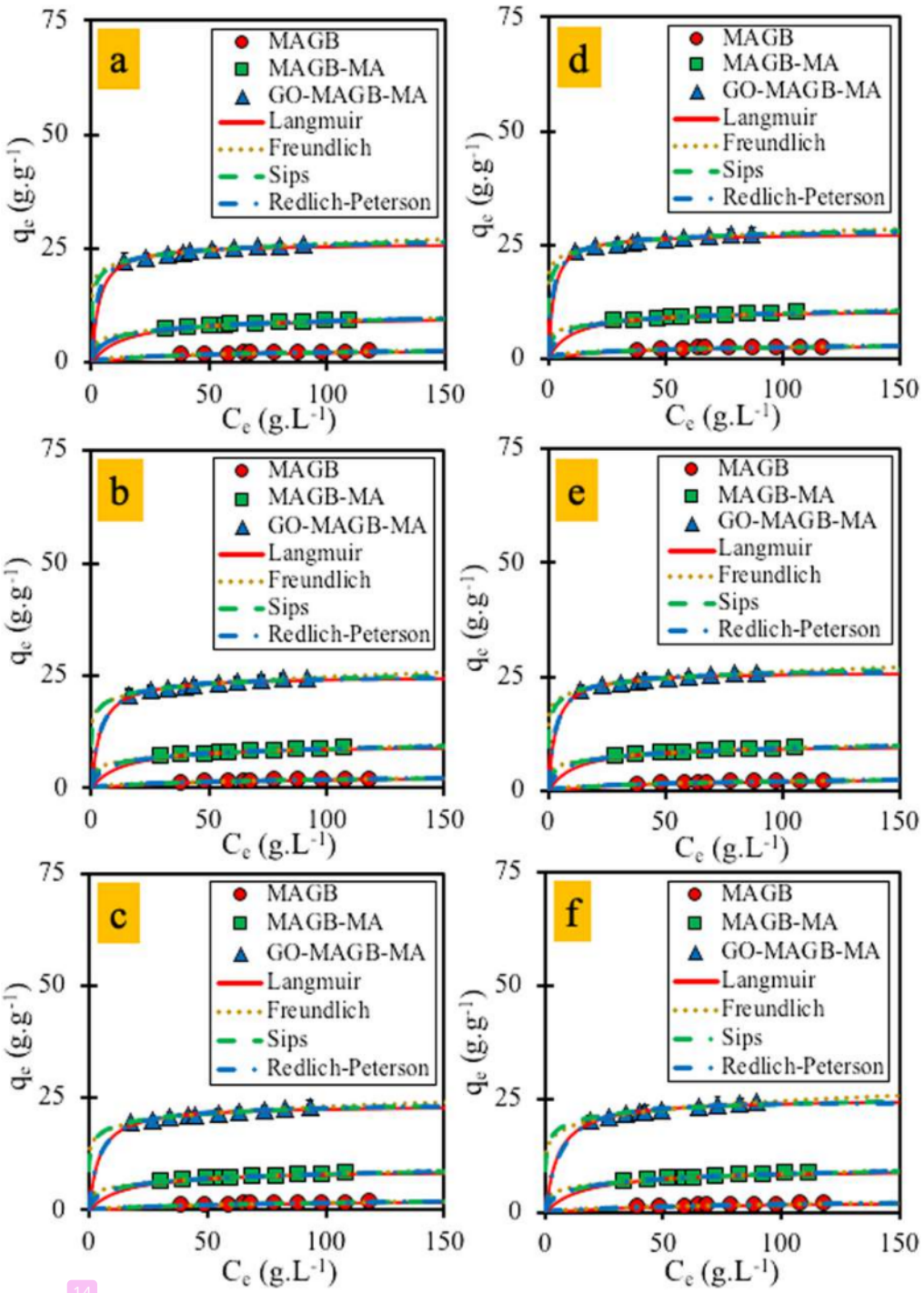


**Fig. 8.** Non-linearized fitting of experimental data to Langmuir, Freundlich, Sips and Redlich–Peterson model for magnetic removal of oil by MAGB, MAGB-MA and GO-MAGB-MA in freshwater at (a) 25 °C, (b) 35 °C (c) 45 °C and in seawater at (d) 25 °C, (e) 35 °C (f) 45 °C (experiment condition: pH 6, adsorbent dose: 1 g L$^{-1}$, t: 2 h, n: 3).

**Table 3**
Kinetics parameters of oil removal by MAGB, MAGB-MA and GO-MAGB-MA obtained from non-linearized pseudo-first, pseudo-second, Elovich and linearized Intraparticle diffusion models in freshwater (FW) and seawater (SW).

| Kinetics | Medium | Parameter | MAGB | MAGB-MA | GO-MAGB-MA |
|---|---|---|---|---|---|
| Pseudo-first order (PFO) | FW | $q^a$ | 2.5226 | 8.7652 | 23.0905 |
| | | $K_{PFO}$[b] | 0.0602 | 0.0842 | 0.0825 |
| | | $R^2$ | 0.9894 | 0.9855 | 0.9850 |
| | | $\chi^2$ | 0.0618 | 0.2285 | 0.5583 |
| | | ARE | 5.1008 | 4.8323 | 4.8874 |
| | SW | $q^a$ | 2.7241 | 9.1900 | 23.9819 |
| | | $K_{PFO}$[b] | 0.0617 | 0.0784 | 0.0772 |
| | | $R^2$ | 0.9917 | 0.9863 | 0.9868 |
| | | $\chi^2$ | 0.0529 | 0.2409 | 0.5144 |
| | | ARE | 4.4541 | 4.9864 | 4.8672 |
| Pseudo-second order (PSO) | FW | $q^a$ | 2.9526 | 9.9405 | 26.2137 |
| | | $K_{PSO}$[c] | 0.0245 | 0.0114 | 0.0042 |
| | | $R^2$ | 0.9999 | 1.0000 | 0.9998 |
| | | $\chi^2$ | 0.0005 | 0.0003 | 0.0069 |
| | | ARE | 0.3990 | 0.1538 | 0.4094 |
| | SW | $q^a$ | 3.1820 | 10.4778 | 27.3931 |
| | | $K_{PSO}$[c] | 0.0234 | 0.0099 | 0.0037 |
| | | $R^2$ | 0.9997 | 0.9999 | 1.0000 |
| | | $\chi^2$ | 0.0012 | 0.0008 | 0.0011 |
| | | ARE | 0.6520 | 0.2391 | 0.1958 |
| Elovich | FW | $\alpha^d$ | 0.4317 | 3.4644 | 8.6973 |
| | | $\beta^e$ | 1.5892 | 0.5559 | 0.2090 |
| | | $R^2$ | 0.9903 | 0.9849 | 0.9852 |
| | | $\chi^2$ | 0.0406 | 0.1907 | 0.4906 |
| | | ARE | 4.4292 | 4.8300 | 4.7915 |
| | SW | $\alpha^d$ | 0.4883 | 3.0089 | 7.4749 |
| | | $\beta^e$ | 1.4879 | 0.5091 | 0.1928 |
| | | $R^2$ | 0.9869 | 0.9857 | 0.9856 |
| | | $\chi^2$ | 0.0576 | 0.1938 | 0.5178 |
| | | ARE | 5.0872 | 4.8032 | 4.8757 |
| Intraparticle Diffusion (IPD) | FW | $K_{1\text{-}IPD}$[f] | 0.3890 | 1.5071 | 3.9222 |
| | | $C_{1\text{-}IPD}$[g] | 0.0126 | 0.1934 | 0.5354 |
| | | $R^2$ | 0.9976 | 0.9910 | 0.9885 |
| | | $K_{2\text{-}IPD}$[f] | 0.1253 | 0.3200 | 0.8797 |
| | | $C_{2\text{-}IPD}$[g] | 1.3508 | 5.9666 | 15.3548 |
| | | $R^2$ | 0.9509 | 0.9454 | 0.9162 |
| | SW | $K_{1\text{-}IPD}$[f] | 0.4271 | 1.5450 | 4.0256 |
| | | $C_{1\text{-}IPD}$[g] | 0.0220 | 0.1542 | 0.3322 |
| | | $R^2$ | 0.9981 | 0.9927 | 0.9936 |
| | | $K_{2\text{-}IPD}$[f] | 0.1253 | 0.3541 | 0.9417 |
| | | $C_{2\text{-}IPD}$[g] | 1.5511 | 6.0430 | 15.5850 |
| | | $R^2$ | 0.9505 | 0.9377 | 0.9454 |

[a] $q_t$ in g $g^{-1}$.
[b] $K_{PFO}$ in $min^{-1}$.
[c] $K_{PSO}$ in g $g^{-1}$ $min^{-1}$.
[d] α in g $g^{-1}$ $min^{-1}$.
[e] β in g $g^{-1}$.
[f] $K_{IPD}$ in g $g^{-1}$ $min^{-0.5}$.
[g] $C_{IPD}$ in g $g^{-1}$.

increase in adsorbed oil. Here, the oil passes through the boundary layer and occupies binding sites on the surfaces of MAGB, MAGB-MA, and GO-MAGB-MA. Adsorption rates are relatively slow in the second stage because of the interparticle diffusion of oil within the pores of MAGB, MAGB-MA, and GO-MAGB-MA; finally, equilibrium is reached. Thus, a two-stage mechanism for oil removal by MAGB, MAGB-MA, and GO-MAGB-MA occurred via surface film adsorption followed by interparticle diffusion. The short time to equilibrium in freshwater and seawater is attractive from a practical and economic point of view, indicating that the application of the as-prepared magnetic hollow beads could be scaled up.

### 3.7.5. Isothermal studies of the effect of GO and MA at different temperatures

Isotherm modeling to understand the relationship between oil adsorption and the adsorption capacity of MAGB, MAGB-MA, and GO-MAGB-MA was carried out. Several isotherms have been developed,

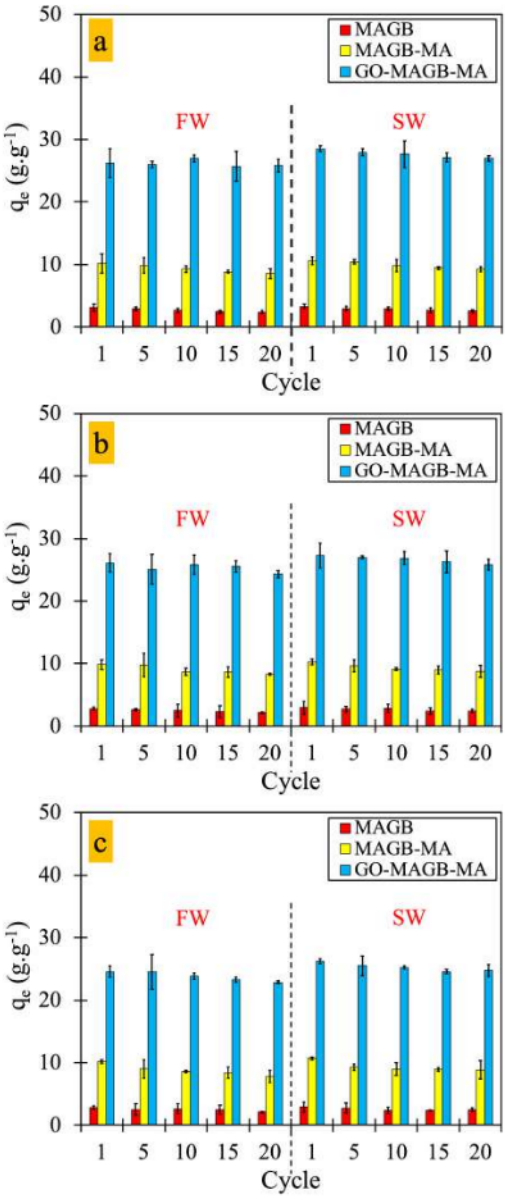


**Fig. 9.** Recycle test of MAGB, MAGB-MA and GO-MAGB-MA for magnetic removal of oil in freshwater (FW) and seawater (SW) at (a) 25 °C, (b) 35 °C, and (c) 45 °C (experiment condition: $C_0$: 100 g $L^{-1}$, t: 2 h, adsorbent dose: 1 g $L^{-1}$and n: 3).

including the two-parameter Langmuir [49] and Freundlich [50] and three-parameters R-P [51] and Sips models. The non-linearized plot of all isotherms are presented in Fig. 5, and the calculated $R^2$, $\chi^2$, and ARE as well as all isotherm parameters are listed in Table S1. The suitability of each model was determined by considering $R^2$, $\chi^2$, and ARE values. At 25 °C, the Freundlich isotherm yielded the highest $R^2$ and lowest $\chi^2$ and ARE values in freshwater and seawater, indicating that oil adsorption occurs via a multilayer mechanism on the heterogenous MAGB-MA and GO-MAGB-MA surfaces. Because of the absence of GO and MA as additional adsorption site, adsorption on the MAGB surface followed the Langmuir model. Overall, based on $R^2$, $\chi^2$, and ARE values, the data fit

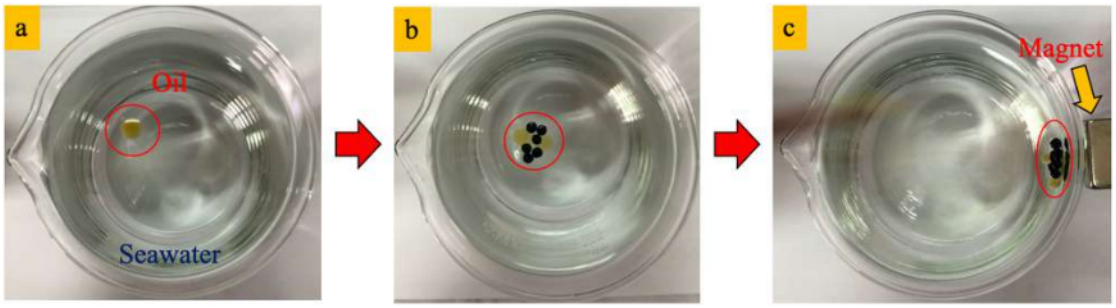


**Fig. 10.** Photograph of (a) oil spill in seawater, (b) oil-GO-MAGB-MA interaction and (c) separation of oil-GO-MAGB-MA by magnet.

the isotherms in order: Freundlich > Sips > Langmuir > Redlich–Peterson (R–P) for MAGB-MA and GO-MAGB-MA. For MAGB, the order is Langmuir > Sips > Freundlich > Redlich–Peterson. Thus, the presence of GO and MA changed the adsorption of the beads from that of a monolayer homogenous system to multilayer heterogenous system.

As the temperature increased from 25 °C to 45 °C, the monolayer capacity of GO-MAGB-MA increased from 26.2276 to 23.5648 and from 27.5285 to 25.2591 g of oil/g of adsorbent in freshwater and seawater, respectively. Similar behavior was observed for MAGB and MAGB-MA. The increase in the adsorption capacity of all the adsorbent beads with increase in temperature is due to (i) the weakening of physical adsorption facilitated by non-electrostatic (hydrophobic) interactions between the beads and oil and (ii) the reduction in oil viscosity, which results in higher solubility of oil in water and the detachment of oil from the adsorbent during magnetic collection. This result is consistent with the behavior of other adsorbents [52,53]. However, even though the adsorption capacity decreased as the temperature increased, the adsorption capacity of GO-MAGB-MA at 45 °C in freshwater and seawater remained higher than those of other reported adsorbents at room temperature. Thus, GO-MAGB-MA is an effective and efficient adsorbent.

### 3.7.6. Practical evaluation

For environmental sustainability, practicality, and economic reasons, collection and regeneration, as well as high $q_{max}$, short $t_{eq}$, and high $M_s$, are crucial. After adsorption, the oil-loaded GO-MAGB-MA remained floating and could be collected using an external magnet, which was rapid and simple because of the high $M_s$ value (Fig. 10). The regeneration of the used GO-MAGB-MA was evaluated over 20 consecutive adsorption–washing–drying cycles in freshwater and seawater. As illustrated in Fig. 9, GO-MAGB-MA maintained a $q_{max}$ of 98% compared to the first run, whereas MAGB and MAGB-MA lost approximately 23% and 15% of their $q_{max}$, respectively. Over 20 adsorption–washing–drying cycles, the flotation, magneto-responsiveness, and adsorptive performance of the GO-MAGB-MA was preserved in freshwater and seawater.

Comparison of GO-MAGB-MA, as well as the MAGB and MAGB-MA, with other reported adsorbents [53–65] were conducted to evaluate the magnetic performance ($M_s$), $t_{eq}$, $q_{max}$, and reusability. GO-MAGB-MA had a relatively higher $q_{max}$ and shorter $t_{eq}$ compared to some adsorbents reported in other works (Table S2). Some other reported adsorbents are superior in terms of $q_{max}$ than GO-MAGB-MA. However, their collection could be challenging because of the lack of magneto-responsiveness or low $M_s$ values. In the case of conventional organic and inorganic adsorbents utilization, adsorbent tend to sink during adsorption of oil and contaminate sea sediment. Some of organic

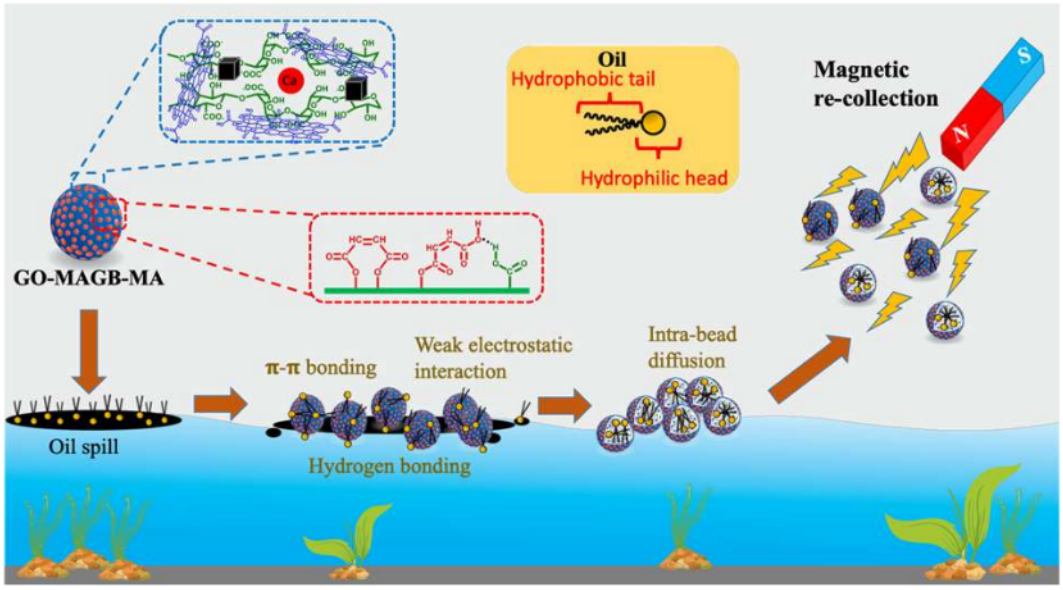


**Scheme 2.** Removal of oil spill on surface of water by the GO-MAGB-MA and its magnetic re-collection.

and inorganic adsorbents also reported to be toxic to the environment make the pollution of become more severe [66]. Smaller size of adsorbent such as in nanoscale size showed affinity toward oil. However, due to its small size, magnetic particle tend to oxidize resulting particle with low magnetization and the re-collection process will be troublesome [67]. The unique combination of buoyancy, high $q_{max}$, and short $t_{eq}$ in freshwater and seawater make GO-MAGB-MA suitable for large-scale oil-contaminated water remediation (see Scheme 2). Adsorbent preparation costs can be minimized because easy and simple collection and regeneration are possible. Moreover, alginate layer protected magnetite core inside the bead so then it can be applied up to 20 cycles without losing its magnetization.

## 4. Conclusions

In this study, self-floating alginate beads were prepared using $CaCO_3$ and $NaHCO_3$ as cavity templates, and $Fe_3O_4$ was incorporated into the hollow structure to yield magnetic beads. The buoyancy and swelling can be improved by the addition of GO following the anchoring of MA. The carbon and oxygen-dominant sheet-like structure of GO was confirmed by SEM-EDX, TEM, AFM, XRD, and Raman analysis. The hollow structure of GO-MAGB-MA was confirmed by SEM and EDX mapping, which showed that C, O, Ca, and Fe were distributed equally on the rough outer surface. The FTIR spectra and TGA results confirmed the presence of 4.14 wt% MA in MAGB-MA and 5.52 wt% MA in GO-MAGB-MA. The average size of MAGB, MAGB-MA and GO-MAGB-MA were $2.93 \pm 0.18$, $3.02 \pm 0.23$, and $3.24 \pm 0.16$ mm with $M_s$ values of 43.268, 43.134, and 26.371 emu $g^{-1}$, respectively, implying strong magneto-responsivity. Oil removal was pH independent at $3 \leq pH \leq 10$ in freshwater and seawater, suggesting a non-electrostatic adsorptive mechanism. Kinetic modeling showed that equilibrium can be achieved within 30 min and initial adsorption is the rate-limiting step, as shown by the good fit to the PSO, having $R^2 \geq 0.9998$, $\chi 2 \leq 0.0069$, and ARE $\leq 0.4094$. The Freundlich isotherm, indicating a multilayer, heterogenous adsorption process, also fit the data well, having $R^2 \geq 0.9966$, $\chi^2 \leq 3.33 \times 10^{-4}$ and ARE $\leq 0.2349$. The presence of GO, MA, and $Fe_3O_4$ means that buoyancy, absorptivity, and magneto-responsiveness are retained even after 20 adsorption–washing cycles. The synergetic combination of pH independent, high adsorption rate and capacity, self-floating, and magneto-responsiveness make GO-MAGB-MA superior in comparation with other published adsorbents in the term of adsorption and re-collection. For future studies, preparation of the GO-MAGB-MA with bigger size maybe carried out to meet large-scale oil spill remediation requirement. Combination with other technology such as skimmer can be also conducted to enhance skimmer performance on oil-spill remediation. The continuous adsorption study by using adsorptive column filled with the GO-MAGB-MA would be great to be conducted for larger-scale remediation especially for emulsified oily water or wastewater.

## CRediT authorship contribution statement

**Satya Candra Wibawa Sakti:** Conceptualization, Methodology, Investigation, Writing-Original Draft. **Rizki Ainuna Wijaya:** Investigation. **Nindayu Indrasari:** Investigation. **Mochamad Zakki Fahmi:** Supervision, Writing-Review & Editing, Funding Acquisition. **Alfa Akustia Widati:** Investigation, Funding acquisition. **Abdulloh:** Investigation, Funding acquisition. **Nuryono:** Supervision **Chun-Hu Chen:** Investigation, Writing-Review & Editing, Funding acquisition.

## Declaration of Competing Interest

The authors declare that they have no known competing financial interests or personal relationships that could have appeared to influence the work reported in this paper.

## Acknowledgments

This project was supported by the Ministry of Research, Technology and Higher Education, Republic of Indonesia through the PDUPT Project with contract No. 714/UN3.14/LT/2019. We also thank Dr. Hwei Voon Lee (Nanotechnology and Catalysis Research Centre, University of Malaya, Malaysia) for her support on VSM measurement. We are very grateful to two anonymous reviewers for their valuable suggestions and comments.

## Appendix A. Supplementary material

Supplementary data associated with this article can be found in the online version at doi:10.1016/j.jece.2020.104935.

## References

[1] Z. Nixon, J. Michel, A review of distribution and quantity of lingering subsurface oil from the Exxon Valdez oil spill, Deep Sea Res. Part II Top. Stud. Oceanogr. 147 (2018) 79–86, https://doi.org/10.1016/j.dsr2.2017.07.009.
[2] J. Beyer, H.C. Trannum, T. Bakke, P.V. Hodson, T.K. Collier, Environmental effects of the deepwater horizon oil spill: a review, Mar. Pollut. Bull. 110 (2016) 28–51, https://doi.org/10.1016/j.marpolbul.2016.06.027.
[3] M.P. Arora, S. Lodhia, The BP Gulf of Mexico oil spill: exploring the link between social and environmental disclosures and reputation risk management, J. Clean. Prod. 140 (2017) 1287–1297, https://doi.org/10.1016/j.jclepro.2016.10.027.
[4] K.A. Colvin, C. Lewis, T.S. Galloway, Current issues confounding the rapid toxicological assessment of oil spills, Chemosphere 245 (2020), 125585, https://doi.org/10.1016/j.chemosphere.2019.125585.
[5] H.D.M. Villela, R.S. Peixoto, A.U. Soriano, F.L. Carmo, Microbial bioremediation of oil contaminated seawater: a survey of patent deposits and the characterization of the top genera applied, Sci. Total Environ. 666 (2019) 743–758, https://doi.org/10.1016/j.scitotenv.2019.02.153.
[6] S.H. Baharuddin, N.A. Mustahil, A.V.B. Reddy, A.A. Abdullah, M.I.A. Mutalib, M. Moniruzzaman, Development, formulation and optimization of a novel biocompatible ionic liquids dispersant for the effective oil spill remediation, Chemosphere 249 (2020), 126125, https://doi.org/10.1016/j.chemosphere.2020.126125.
[7] A. Abidli, Y. Huang, P. Cherukupally, A.M. Bilton, C.B. Park, Novel separator skimmer for oil spill cleanup and oily wastewater treatment: from conceptual system design to the first pilot-scale prototype development, Environ. Technol. Innov. 18 (2020), 100598, https://doi.org/10.1016/j.eti.2019.100598.
[8] Y. Shi, J. Wei, S. Li, S. Peng, B. Zhang, Experimental study on containment of moderate-viscous oil by floating boom subject to waves and currents, Appl. Ocean Res. 94 (2020), 102003, https://doi.org/10.1016/j.apor.2019.102003.
[9] R.J. Bullock, R.A. Perkins, S. Aggarwal, In-situ burning with chemical herders for Arctic oil spill response: meta-analysis and review, Sci. Total Environ. 675 (2019) 705–716, https://doi.org/10.1016/j.scitotenv.2019.04.127.
[10] L. Abou Chacra, M.A. Sabri, T.H. Ibrahim, M.I. Khamis, N.M. Hamdan, S. Al-Asheh, M. Alrefai, C. Fernandez, Application of graphene nanoplatelets and graphene magnetite for the removal of emulsified oil from produced water, J. Environ. Chem. Eng. 6 (2018) 3018–3033, https://doi.org/10.1016/j.jece.2018.04.060.
[11] A.K. Singh, K. Ketan, J.K. Singh, Simple and green fabrication of recyclable magnetic highly hydrophobic sorbents derived from waste orange peels for removal of oil and organic solvents from water surface, J. Environ. Chem. Eng. 5 (2017) 5250–5259, https://doi.org/10.1016/j.jece.2017.09.060.
[12] J. Ma, M. Xia, S. Zhu, F. Wang, A new alendronate doped HAP nanomaterial for $Pb^{2+}$, $Cu^{2+}$ and $Cd^{2+}$ effect absorption, J. Hazard. Mater. 400 (2020), 123143, https://doi.org/10.1016/j.jhazmat.2020.123143.
[13] S. Zhu, M. Asim Khan, F. Wang, Z. Bano, M. Xia, Rapid removal of toxic metals $Cu^{2+}$ and $Pb^{2+}$ by amino trimethylene phosphonic acid intercalated layered double hydroxide: a combined experimental and DFT study, Chem. Eng. J. 392 (2020), 123711, https://doi.org/10.1016/j.cej.2019.123711.
[14] S.C.W. Sakti, R.N. Laily, S. Aliyah, N. Indrasari, M.Z. Fahmi, H.V. Lee, Y. Akemoto, S. Tanaka, Re-collectable and recyclable epichlorohydrin-crosslinked humic acid with spinel cobalt ferrite core for simple magnetic removal of cationic triarylmethane dyes in polluted water, J. Environ. Chem. Eng. 8 (2020), 104004, https://doi.org/10.1016/j.jece.2020.104004.
[15] B. Doshi, E. Repo, J.P. Heiskanen, J.A. Sirviö, M. Sillanpää, Sodium salt of oleoyl carboxymethyl chitosan: a sustainable adsorbent in the oil spill treatment, J. Clean. Prod. 170 (2018) 339–350, https://doi.org/10.1016/j.jclepro.2017.09.163.
[16] K.G. Akpomie, C.F. Onyeabor, C.C. Ezeofor, J.U. Ani, S.I. Eze, Natural aluminosilicate clay obtained from south-eastern Nigeria as potential sorbent for oil spill remediation, J. Afr. Earth Sci. 155 (2019) 118–123, https://doi.org/10.1016/j.jafrearsci.2019.04.013.
[17] W. Du, X. Wang, G. Chen, J. Zhang, M. Slaný, Synthesis, property and mechanism analysis of a novel polyhydroxy organic amine shale hydration inhibitor, Minerals 10 (2020) 128, https://doi.org/10.3390/min10020128.
[18] K. AlAmeri, A. Giwa, L. Yousef, A. Alraeesi, H. Taher, Sorption and removal of crude oil spills from seawater using peat-derived biochar: an optimization study,

J. Environ. Manag. 250 (2019), 109465, https://doi.org/10.1016/j.jenvman.2019.109465.
[19] B. Doshi, M. Sillanpää, S. Kalliola, A review of bio-based materials for oil spill treatment, Water Res. 135 (2018) 262–277, https://doi.org/10.1016/j.watres.2018.02.034.
[20] R. Hummers, W. S, E. Offeman, Preparation of graphitic oxide, J. Am. Chem. Soc. 208 (1957) 1937. ⟨https://pubs.acs.org/sharingguidelines⟩.
[21] Y. Hou, S. Lv, L. Liu, X. Liu, High-quality preparation of graphene oxide via the Hummers' method: Understanding the roles of the intercalator, oxidant, and graphite particle size, Ceram. Int. 46 (2020) 2392–2402, https://doi.org/10.1016/j.ceramint.2019.09.231.
[22] J. Park, Y.S. Cho, S.J. Sung, M. Byeon, S.J. Yang, C.R. Park, Characteristics tuning of graphene-oxide-based-graphene to various end-uses, Energy Storage Mater. 14 (2018) 8–21, https://doi.org/10.1016/j.ensm.2018.02.013.
[23] M.S. Chang, Y.S. Kim, J.H. Kang, J. Park, S.J. Sung, S.H. So, K.T. Park, S.J. Yang, T. Kim, C.R. Park, Guidelines for tailored chemical functionalization of graphene, Chem. Mater. 29 (2017) 307–318, https://doi.org/10.1021/acs.chemmater.6b02885.
[24] V.D. Ebajo, C.R.L. Santos, G.V. Alea, Y.A. Lin, C.H. Chen, Regenerable acidity of graphene oxide in promoting multicomponent organic synthesis, Sci. Rep. 9 (2019) 1–12, https://doi.org/10.1038/s41598-019-51833-2.
[25] Y. Mao, Q. Huang, B. Meng, K. Zhou, G. Liu, A. Gugliuzza, E. Drioli, W. Jin, Roughness-enhanced hydrophobic graphene oxide membrane for water desalination via membrane distillation, J. Membr. Sci. 611 (2020), 118364, https://doi.org/10.1016/j.memsci.2020.118364.
[26] T.J.M. Fraga, M.G. Ghislandi, M.N. Carvalho, M.A. da Motta Sobrinho, One step forward: how can functionalization enhance the adsorptive properties of graphene towards metallic ions and dyes? Environ. Res. 184 (2020), 109362 https://doi.org/10.1016/j.envres.2020.109362.
[27] N. Baig, Ihsanullah, M. Sajid, T.A. Saleh, Graphene-based adsorbents for the removal of toxic organic pollutants: a review, J. Environ. Manag. 244 (2019) 370–382, https://doi.org/10.1016/j.jenvman.2019.05.047.
[28] J. Yang, L. Zhou, F. Ma, H. Zhao, F. Deng, S. Pi, A. Tang, A. Li, Magnetic nanocomposite microbial extracellular polymeric substances@Fe3O4 supported nZVI for Sb(V) reduction and adsorption under aerobic and anaerobic conditions, Environ. Res. 189 (2020), 109950, https://doi.org/10.1016/j.envres.2020.109950.
[29] T. Madrakian, A. Afkhami, M. Ahmadi, Adsorption and kinetic studies of seven different organic dyes onto magnetite nanoparticles loaded tea waste and removal of them from wastewater samples, Spectrochim. Acta Part A Mol. Biomol. Spectrosc. 99 (2012) 102–109, https://doi.org/10.1016/j.saa.2012.09.025.
[30] M.L. Iordache, G. Dodi, D. Hritcu, D. Draganescu, O. Chiscan, M.I. Popa, Magnetic chitosan grafted (alkyl acrylate) composite particles: synthesis, characterization and evaluation as adsorbents, Arab. J. Chem. 11 (2018) 1032–1043, https://doi.org/10.1016/j.arabjc.2015.12.010.
[31] Q. Wang, S.M. Shaheen, Y. Jiang, R. Li, M. Slaný, H. Abdelrahman, E. Kwon, N. Bolan, J. Rinklebe, Z. Zhang, Fe/Mn- and P-modified drinking water treatment residuals reduced Cu and Pb phytoavailability and uptake in a mining soil, J. Hazard. Mater. 403 (2021), 123628, https://doi.org/10.1016/j.jhazmat.2020.123628.
[32] Y. Narita, S.C.W. Sakti, Y. Akemoto, S. Tanaka, Ultra-rapid removal of cationic organic dyes by novel single- and double-stranded DNA immobilized on quaternary ammonium magnetic chitosan, J. Environ. Chem. Eng. 7 (2019), 103308, https://doi.org/10.1016/j.jece.2019.103308.
[33] S. Nuryono, A. Mighfar, S.C.W. Kuncaka Sakti, Functionalization of Fe3O4/SiO2 with N-(2-aminoethyl)-3-aminopropyl for sorption of [AuCl4]-, Indones. J. Chem. 16 (2016) 130–137. ⟨https://jurnal.ugm.ac.id/ijc/article/view/21155⟩.
[34] W. Du, M. Slaný, X. Wang, G. Chen, J. Zhang, The inhibition property and mechanism of a novel low molecular weight zwitterionic copolymer for improving wellbore stability, Polymers 12 (2020) 708, https://doi.org/10.3390/polym12030708.
[35] E. Hambali, S.C.W. Sakti, M.Z. Fahmi, F.E. Wahyudianto, Nuryono, P. Yessi, M. Yani, E. Sinurat, B.S. Pratama, Effect of extraction time and $Na_2CO_3$ concentration on the characteristics of alginate extracted from sargassum sp, IOP Conf. Ser. Earth Environ. Sci. 209 (2018), 012033, https://doi.org/10.1088/1755-1315/209/1/012033.
[36] M. S, V.K. M, A.D. Tripathi, R.L. TS, Optimization and characterization of Alginic acid synthesized from a novel strain of Pseudomonas stutzeri, Biotechnol. Rep. 27 (2020), e00517, https://doi.org/10.1016/j.btre.2020.e00517.
[37] L. Cao, W. Lu, A. Mata, K. Nishinari, Y. Fang, Egg-box model-based gelation of alginate and pectin: a review, Carbohydr. Polym. 242 (2020), 116389, https://doi.org/10.1016/j.carbpol.2020.116389.
[38] C.H. Chen, S. Hu, J.F. Shih, C.Y. Yang, Y.W. Luo, R.H. Jhang, C.M. Chiang, Y. J. Hung, Effective synthesis of highly oxidized graphene oxide that enables wafer-scale nanopatterning: preformed acidic oxidizing medium approach, Sci. Rep. 7 (2017) 1–10, https://doi.org/10.1038/s41598-017-04139-0.
[39] M. Slaný, Ľ. Jankovič, J. Madejová, Structural characterization of organo-montmorillonites prepared from a series of primary alkylamines salts: mid-IR and near-IR study, Appl. Clay Sci. 176 (2019) 11–20, https://doi.org/10.1016/j.clay.2019.04.016.
[40] X. Lv, Y. Zhang, W. Fu, J. Cao, J. Zhang, H. Ma, G. Jiang, Zero-valent iron nanoparticles embedded into reduced graphene oxide-alginate beads for efficient chromium (VI) removal, J. Colloid Interface Sci. 506 (2017) 633–643, https://doi.org/10.1016/j.jcis.2017.07.024.
[41] J. Li, J. Ma, S. Chen, Y. Huang, J. He, Adsorption of lysozyme by alginate/graphene oxide composite beads with enhanced stability and mechanical property, Mater. Sci. Eng. C 89 (2018) 25–32, https://doi.org/10.1016/j.msec.2018.03.023.
[42] T.P. Armedya, M.F. Dzikri, S.C.W. Sakti, A. Abdulloh, Y. Raharjo, S. Wafiroh, Purwati, M.Z. Fahmi, Kinetical release study of copper ferrite nanoparticle incorporated on PCL/collagen nanofiber for naproxen delivery, Bionanoscience 9 (2019) 274–284, https://doi.org/10.1007/s12668-019-00618-y.
[43] Y. Zhuang, F. Yu, H. Chen, J. Zheng, J. Ma, J. Chen, Alginate/graphene double-network nanocomposite hydrogel beads with low-swelling, enhanced mechanical properties, and enhanced adsorption capacity, J. Mater. Chem. A 4 (2016) 10885–10892, https://doi.org/10.1039/C6TA02738E.
[44] A. Diraki, H.R. Mackey, G. Mckay, A. Abdala, Removal of emulsified and dissolved diesel oil from high salinity wastewater by adsorption onto graphene oxide, J. Environ. Chem. Eng. 7 (2019), 103106, https://doi.org/10.1016/j.jece.2019.103106.
[45] S. Lagergren, About the theory of so-called adsorption of soluble substance, K. Sven. Vetensk. Handl. 24 (1898) 1–39.
[46] Y. Ho, The kinetics of sorption of divalent metal ions onto sphagnum moss peat, Water Res. 34 (2000) 735–742, https://doi.org/10.1016/S0043-1354(99)00232-8.
[47] S.Y. Elovich, O.G. Larionov, Theory of adsorption from solutions of non electrolytes on solid (I) equation adsorption from solutions and the analysis of its simplest form, (II) verification of the equation of adsorption isotherm from solutions, Izv. Akad. Nauk SSSR Otd. Khimicheskikh Nauk 2 (1962) 209–216.
[48] W.J. Weberr, J.C. Moris, Kinetics of adsorption on carbon from solution, J. Sanit. Eng. Div. 89 (1963) 31–60.
[49] I. Langmuir, The adsorption of gases on plane surfaces of glass, mica and platinum, J. Am. Chem. Soc. 40 (1918) 1361–1403, https://doi.org/10.1021/ja02242a004.
[50] H.M. Freundlich, Uber die adsorption in losungen, Z. Phys. Chem. 57 (1906) 385–470.
[51] O. Redlich, D.L. Peterson, A useful adsorption isotherm, J. Phys. Chem. 63 (1959) 1024–1026.
[52] M.A. Mahmoud, Oil spill cleanup by raw flax fiber: modification effect, sorption isotherm, kinetics and thermodynamics, Arab. J. Chem. 13 (2020) 5553–5563, https://doi.org/10.1016/j.arabjc.2020.02.014.
[53] B. Zhang, R. Hu, D. Sun, T. Wu, Y. Li, Fabrication of magnetite-graphene oxide/MgAl-layered double hydroxide composites for efficient removal of emulsified oils from various oil-in-water emulsions, J. Chem. Eng. Data 63 (2018) 4689–4702, https://doi.org/10.1021/acs.jced.8b00739.
[54] H. Wang, K.Y. Lin, B. Jing, G. Krylova, G.E. Sigmon, P. McGinn, Y. Zhu, C. Na, Removal of oil droplets from contaminated water using magnetic carbon nanotubes, Water Res. 47 (2013) 4198–4205, https://doi.org/10.1016/j.watres.2013.02.056.
[55] M. Anju, N.K. Renuka, Magnetically actuated graphene coated polyurethane foam as potential sorbent for oils and organics, Arab. J. Chem. 13 (2020) 1752–1762, https://doi.org/10.1016/j.arabjc.2018.01.012.
[56] O. Guselnikova, A. Barras, A. Addad, E. Sviridova, S. Szunerits, P. Postnikov, R. Boukherroub, Magnetic polyurethane sponge for efficient oil adsorption and separation of oil from oil-in-water emulsions, Sep. Purif. Technol. 240 (2020), 116627, https://doi.org/10.1016/j.seppur.2020.116627.
[57] M. Nazhipkyzy, A. Nurgain, M. Florent, A. Policicchio, T.J. Bandosz, Magnetic soot: surface properties and application to remove oil contamination from water, J. Environ. Chem. Eng. 7 (2019), 103074, https://doi.org/10.1016/j.jece.2019.103074.
[58] N. Wang, Y. Zhang, F. Zhu, J. Li, S. Liu, P. Na, Adsorption of soluble oil from water to graphene, Environ. Sci. Pollut. Res. 21 (2014) 6495–6505, https://doi.org/10.1007/s11356-014-2504-9.
[59] O. Bagoole, M.M. Rahman, S. Shah, H. Hong, H. Chen, A. Al Ghaferi, H. Younes, Functionalized three-dimensional graphene sponges for highly efficient crude and diesel oil adsorption, Environ. Sci. Pollut. Res. 25 (2018) 23091–23105, https://doi.org/10.1007/s11356-018-2248-z.
[60] Z. Rahmani, A.M. Rashidi, A. Kazemi, M.T. Samadi, A.R. Rahmani, N-doped reduced graphene oxide aerogel for the selective adsorption of oil pollutants from water: isotherm and kinetic study, J. Ind. Eng. Chem. 61 (2018) 416–426, https://doi.org/10.1016/j.jiec.2017.12.041.
[61] Z. Rahmani, M. Shafiei-Alavijeh, A. Kazemi, A.M. Rashidi, Synthesis of MIL-101@nanoporous graphene composites as hydrophobic adsorbents for oil removal, J. Taiwan Inst. Chem. Eng. 91 (2018) 597–608, https://doi.org/10.1016/j.jtice.2018.06.015.
[62] S. Songsaeng, P. Thamyongkit, S. Poompradub, Natural rubber/reduced-graphene oxide composite materials: morphological and oil adsorption properties for treatment of oil spills, J. Adv. Res. 20 (2019) 79–89, https://doi.org/10.1016/j.jare.2019.05.007.
[63] S. Javadian, M. khalilifard, S.M. Sadrpoor, Functionalized graphene oxide with core-shell of $Fe_3O_4$@oliec acid nanospheres as a recyclable demulsifier for effective removal of emulsified oil from oily wastewater, J. Water Process Eng. 32 (2019), 100961, https://doi.org/10.1016/j.jwpe.2019.100961.
[64] A. Fossati, M. Martins Alho, S.E. Jacobo, Covalent functionalized magnetic nanoparticles for crude oil recovery, Mater. Chem. Phys. 238 (2019), 121910, https://doi.org/10.1016/j.matchemphys.2019.121910.
[65] X. Lv, D. Tian, Y. Peng, J. Li, G. Jiang, Superhydrophobic magnetic reduced graphene oxide-decorated foam for efficient and repeatable oil-water separation, Appl. Surf. Sci. 466 (2019) 937–945, https://doi.org/10.1016/j.apsusc.2018.10.110.
[66] H. Singh, N. Bhardwaj, S.K. Arya, M. Khatri, Environmental impacts of oil spills and their remediation by magnetic nanomaterials, Environ. Nanotechnol. Monit. Manag. 14 (2020), 100305, https://doi.org/10.1016/j.enmm.2020.100305.

[67] K. Qiao, W. Tian, J. Bai, L. Wang, J. Zhao, Z. Du, X. Gong, Application of magnetic adsorbents based on iron oxide nanoparticles for oil spill remediation: a review, J. Taiwan Inst. Chem. Eng. 97 (2019) 227–236, https://doi.org/10.1016/j.jtice.2019.01.029.

[68] N. Nuryono, D. Miswanda, S.C.W. Sakti, B. Rusdiarso, P.A. Krisbiantoro, N. Utami, R. Otomo, Y. Kamiya, Chitosan-functionalized natural magnetic particle@silica modified with (3-chloropropyl)trimethoxysilane as a highly stable magnetic adsorbent for gold(III) ion, Mater. Chem. Phys. 255 (2020), 123507, https://doi.org/10.1016/j.matchemphys.2020.123507.

[69] S.C.W. Sakti, Y. Narita, T. Sasaki, N. Nuryono, S. Tanaka, A novel pyridinium functionalized magnetic chitosan with pH-independent and rapid adsorption kinetics for magnetic separation of Cr(VI), J. Environ. Chem. Eng. 3 (3) (2015) 1953–1961, https://doi.org/10.1016/j.jece.2015.05.004.

# Magnetic hollow buoyant alginate beads achieving rapid remediation of oil contamination on water

ORIGINALITY REPORT

| 11% | 6% | 9% | 2% |
|---|---|---|---|
| SIMILARITY INDEX | INTERNET SOURCES | PUBLICATIONS | STUDENT PAPERS |

PRIMARY SOURCES

| | | |
|---|---|---|
| 1 | Hyeongoo Kim, Gang Zhang, Min Wu, Jinshan Guo, Changwoo Nam. "Highly Efficient and Recyclable Polyolefin-based Magnetic Sorbent for Oils and Organic Solvents Spill Cleanup", Journal of Hazardous Materials, 2021<br>Publication | 2% |
| 2 | Nuryono Nuryono, Dikki Miswanda, Satya Candra Wibawa Sakti, Bambang Rusdiarso et al. "Chitosan-functionalized natural magnetic particle@silica modified with (3-chloropropyl)trimethoxysilane as a highly stable magnetic adsorbent for gold(III) ion", Materials Chemistry and Physics, 2020<br>Publication | 1% |
| 3 | repositorio.ipen.br<br>Internet Source | <1% |
| 4 | eprints.lmu.edu.ng<br>Internet Source | <1% |
| 5 | Wyllamanney da S. Pereira, Fabrício B. Destro, Cipriano B. Gozzo, Edson R. Leite, Júlio C. | <1% |

Sczancoski. "Insight into the enhanced photocatalytic properties of AgBr/Ag4P2O7 composites synthesized via in situ ion exchange reaction", Journal of Environmental Chemical Engineering, 2021
Publication

| | | |
|---|---|---|
| 6 | myresearchspace.uws.ac.uk<br>Internet Source | <1 % |
| 7 | scholarbank.nus.edu.sg<br>Internet Source | <1 % |
| 8 | Arun K. Singh, Kumar Ketan, Jayant K. Singh. "Simple and green fabrication of recyclable magnetic highly hydrophobic sorbents derived from waste orange peels for removal of oil and organic solvents from water surface", Journal of Environmental Chemical Engineering, 2017<br>Publication | <1 % |
| 9 | academic.hep.com.cn<br>Internet Source | <1 % |
| 10 | Mi Se Chang, Yern Seung Kim, Jong Hun Kang, Jisoo Park et al. "Guidelines for Tailored Chemical Functionalization of Graphene", Chemistry of Materials, 2016<br>Publication | <1 % |
| 11 | s-space.snu.ac.kr<br>Internet Source | <1 % |

| | | |
|---|---|---|
| 12 | Tao Tian, Zhishan Bai, Bingjie Wang, Shenghao Zhao, Yong Zhang. "Facile fabrication of polyacrylic acid functionalized carboxymethyl chitosan microspheres for selective and efficient removal of Ni(II) from multicomponent wastewater", Colloids and Surfaces A: Physicochemical and Engineering Aspects, 2020<br>Publication | <1 % |
| 13 | fcee.utm.my<br>Internet Source | <1 % |
| 14 | Nikolina A. Travlou, George Z. Kyzas, Nikolaos K. Lazaridis, Eleni A. Deliyanni. "Functionalization of Graphite Oxide with Magnetic Chitosan for the Preparation of a Nanocomposite Dye Adsorbent", Langmuir, 2013<br>Publication | <1 % |
| 15 | jurnal.ugm.ac.id<br>Internet Source | <1 % |
| 16 | Billie Yan Zhang Hiew, Lai Yee Lee, Xin Jiat Lee, Suchithra Thangalazhy-Gopakumar et al. "Review on synthesis of 3D graphene-based configurations and their adsorption performance for hazardous water pollutants", Process Safety and Environmental Protection, 2018<br>Publication | <1 % |

| | | |
|---|---|---|
| 17 | Harpreet Singh, Neha Bhardwaj, Shailendra Kumar Arya, Madhu Khatri. "Environmental impacts of oil spills and their remediation by magnetic nanomaterials", Environmental Nanotechnology, Monitoring & Management, 2020<br>Publication | <1 % |
| 18 | Jiwei Li, Jianwei Ma, Shaojuan Chen, Yudong Huang, Jinmei He. "Adsorption of lysozyme by alginate/graphene oxide composite beads with enhanced stability and mechanical property", Materials Science and Engineering: C, 2018<br>Publication | <1 % |
| 19 | Mahima Sharma, Monika Joshi, Subhasha Nigam, Devesh Kumar Avasthi et al. "Efficient oil removal from wastewater based on polymer coated superhydrophobic tetrapodal magnetic nanocomposite adsorbent", Applied Materials Today, 2019<br>Publication | <1 % |
| 20 | core.ac.uk<br>Internet Source | <1 % |
| 21 | www.journaltocs.ac.uk<br>Internet Source | <1 % |
| 22 | Mochamad Zakki Fahmi, Roch Adi Prasetya, Muhammad Fathan Dzikri, Satya Candra | <1 % |

Wibawa Sakti et al. "MnFe2O4 nanoparticles/cellulose acetate composite nanofiber for controllable release of naproxen", Materials Chemistry and Physics, 2020
Publication

---

23 Azizi, Avideh, Ali Torabian, Elham Moniri, Amir Hessam Hassani, and Homayon Ahmad Panahi. "Adsorption performance of modified graphene oxide nanoparticles for the removal of toluene, ethylbenzene, and xylenes from aqueous solution", Desalination and Water Treatment, 2016.
Publication

<1 %

---

24 Monika Bil, Ewa Kijeńska-Gawrońska, Eliza Głodkowska-Mrówka, Aneta Manda-Handzlik, Piotr Mrówka. "Design and in vitro evaluation of electrospun shape memory polyurethanes for self-fitting tissue engineering grafts and drug delivery systems", Materials Science and Engineering: C, 2020
Publication

<1 %

---

25 Abbas Mohammadi, Amir Hossein Doctorsafaei, Khalid Mahmood Zia. "Alginate/calix[4]arenes modified graphene oxide nanocomposite beads: Preparation, characterization, and dye adsorption studies",

<1 %

International Journal of Biological Macromolecules, 2018
Publication

| | | |
|---|---|---|
| 26 | Jingjing Yao, Yi Deng, Siyuan Pan, Ramon Korna, Jiayi Wen, Nadi Yuan, Kun Wang, Haipu Li, Ying Yang. "The difference in the adsorption mechanisms of magnetic ferrites modified carbon nanotubes", Journal of Hazardous Materials, 2021<br>Publication | <1 % |
| 27 | Zhaohong Xu, Qi Zhu, Jumeng Bian. "Preparation of a recyclable demulsifier for the treatment of emulsified oil wastewater by chitosan modification and sodium oleate grafting Fe3O4", Journal of Environmental Chemical Engineering, 2021<br>Publication | <1 % |
| 28 | pub.uni-bielefeld.de<br>Internet Source | <1 % |
| 29 | ro.uow.edu.au<br>Internet Source | <1 % |
| 30 | www.akademiabaru.com<br>Internet Source | <1 % |
| 31 | André Segadas Figueiredo, Luis Peña Icart, Fernanda Davi Marques, Edson Rodrigo Fernandes et al. "Extrinsically magnetic poly(butylene succinate): An up-and-coming | <1 % |

| | | |
|---|---|---|
| | petroleum cleanup tool", Science of The Total Environment, 2019<br>Publication | |
| 32 | Perez-Marin, A.B.. "Removal of cadmium from aqueous solutions by adsorption onto orange waste", Journal of Hazardous Materials, 20070102<br>Publication | <1 % |
| 33 | bmcbioinformatics.biomedcentral.com<br>Internet Source | <1 % |
| 34 | en.unionpedia.org<br>Internet Source | <1 % |
| 35 | ourarchive.otago.ac.nz<br>Internet Source | <1 % |
| 36 | www.dovepress.com<br>Internet Source | <1 % |
| 37 | www.preprints.org<br>Internet Source | <1 % |
| 38 | Aseel M. Aljeboree, Ayad F. Alkaim, Ammar H. Al-Dujaili. "Adsorption isotherm, kinetic modeling and thermodynamics of crystal violet dye on coconut husk-based activated carbon", Desalination and Water Treatment, 2014<br>Publication | <1 % |

| | | |
|---|---|---|
| 39 | Gabriel V.S. Dutra, Olacir A. Araújo, Weslany S. Neto, Vijayendra K. Garg, Aderbal C. Oliveira, Adolfo F. Júnior. "Obtaining superhydrophopic magnetic nanoparticles applicable in the removal of oils on aqueous surface", Materials Chemistry and Physics, 2017<br>Publication | <1 % |
| 40 | K. Rambabu, Jawaher AlYammahi, G. Bharath, A. Thanigaivelan, N. Sivarajasekar, Fawzi Banat. "Nano-activated carbon derived from date palm coir waste for efficient sequestration of noxious 2,4-dichlorophenoxyacetic acid herbicide", Chemosphere, 2021<br>Publication | <1 % |
| 41 | Qiyun Zhang, Ting Cheng, Qilang Lin, Changqing Fang. "Facile preparation of robust dual MgO-loaded carbon foam as an efficient adsorbent for malachite green removal", Environmental Research, 2021<br>Publication | <1 % |
| 42 | Submitted to Universitas Negeri Semarang<br>Student Paper | <1 % |
| 43 | Submitted to University of Central Florida<br>Student Paper | <1 % |
| 44 | Www.mdpi.com<br>Internet Source | <1 % |

| | | |
|---|---|---|
| 45 | biomedres.us<br>Internet Source | <1 % |
| 46 | dokumen.pub<br>Internet Source | <1 % |
| 47 | m.scirp.org<br>Internet Source | <1 % |
| 48 | openhub.spu.ac.za<br>Internet Source | <1 % |
| 49 | watersa.net<br>Internet Source | <1 % |
| 50 | www.jim.or.jp<br>Internet Source | <1 % |
| 51 | www.mrforum.com<br>Internet Source | <1 % |
| 52 | A.M.P. Madhubashani, Dimitrios A. Giannakoudakis, B.M.W.P.K. Amarasinghe, Anushka Upamali Rajapaksha et al. "Propensity and appraisal of biochar performance in removal of oil spills: A comprehensive review", Environmental Pollution, 2021<br>Publication | <1 % |
| 53 | Haihua Xu, Sidi Zhu, Mingzhu Xia, Fengyun Wang. "Rapid and efficient removal of diclofenac sodium from aqueous solution via | <1 % |

ternary core-shell CS@PANI@LDH composite: Experimental and adsorption mechanism study", Journal of Hazardous Materials, 2021
Publication

| | | |
|---|---|---|
| 54 | Ivo Safarik, Eva Baldikova, Jitka Prochazkova, Mirka Safarikova, Kristyna Pospiskova. "Magnetically Modified Agricultural and Food Waste: Preparation and Application", Journal of Agricultural and Food Chemistry, 2018<br>Publication | <1 % |
| 55 | Parisa Hoshyarmanesh, Zahra Mohammadbagheri, Abbas Rahmati. "Synthesis and application of bisurea derivatives: Effect of structural differences on the gelation properties", Journal of Environmental Chemical Engineering, 2021<br>Publication | <1 % |
| 56 | baadalsg.inflibnet.ac.in<br>Internet Source | <1 % |
| 57 | fjps.springeropen.com<br>Internet Source | <1 % |
| 58 | gulfresearchinitiative.org<br>Internet Source | <1 % |
| 59 | www.scielo.br<br>Internet Source | <1 % |
| 60 | www.springerprofessional.de<br>Internet Source | <1 % |

| | | |
|---|---|---|
| 61 | Ewa Knapik. "Biodemulsification combined with fixed-bed biosorption for the recovery of crude oil from produced water", Journal of Water Process Engineering, 2020<br>Publication | <1 % |
| 62 | Karna Wijaya, Muhammad Ahan Kurniawan, Wahyu Dita Saputri, Wega Trisunaryanti et al. "Synthesis of Nickel Catalyst Supported on ZrO2/SO4 Pillared Bentonite and Its Application for Conversion of Coconut Oil into Gasoline via Hydrocracking Process", Journal of Environmental Chemical Engineering, 2021<br>Publication | <1 % |
| 63 | Ali Khadir, Mahsa Motamedi, Ebrahim Pakzad, Mika Sillanpää, Shreya Mahajan. "The prospective utilization of Luffa fibres as a lignocellulosic bio-material for environmental remediation of aqueous media: A review", Journal of Environmental Chemical Engineering, 2020<br>Publication | <1 % |
| 64 | Yonggang Hou, Shenghua Lv, Leipeng Liu, Xiang Liu. "High-quality preparation of graphene oxide via the Hummers' method: Understanding the roles of the intercalator, oxidant, and graphite particle size", Ceramics International, 2020<br>Publication | <1 % |

| | | | |
|---|---|---|---|
| Exclude quotes | On | Exclude matches | < 5 words |
| Exclude bibliography | On | | |

# Magnetic hollow buoyant alginate beads achieving rapid remediation of oil contamination on water

GRADEMARK REPORT

FINAL GRADE

/0

GENERAL COMMENTS

**Instructor**

PAGE 1

PAGE 2

PAGE 3

PAGE 4

PAGE 5

PAGE 6

PAGE 7

PAGE 8

PAGE 9

PAGE 10

PAGE 11

PAGE 12

PAGE 13

PAGE 14

PAGE 15

PAGE 16